Final response

We thank both referees for their thorough review of our paper and the evaluation of the formulation of the dry deposition scheme. In consideration of all comments, it became necessary to revise a major part of the dry deposition implementation in our model. Particularly, we

- have addressed and corrected the equations in
  - the implementation of the mosaic approach,
  - the computation of R_a.
- have fixed the equations with respect to comprehensibility (e.g., indexing),
- have included a diagnostic output of dry deposition velocities,
- now refer to our new dry deposition scheme as *mOSaic scheme*,
- have refined the definition of our model experiments to make them more consistent, especially
  - using the soil moisture at a more appropriate level (SWVL3) and
  - CEDS emissions in accordance to the meteorological year.

  This also includes replacement or removal of some previous experiments
  - *EMEP_SWVL4* $\rightarrow$ *mOSaic_SWVL1*,
  - ~~*EMEP_ppgs*~~,
  - ~~*EMEP_ppgssh*~~, and
  - *EMEP_ppgs_2005* $\rightarrow$ *mOSaic_emis2014*.

  We have added two experiments in which we explicitly change the prescribed ozone surface resistance $R^{\mathrm{O_3}}$:
  - *mOSaic_desert*,
  - *mOSaic_hough*.
- have elaborated on the evaluation and discussion of the results and
- included a section in which we compare our results to the MACC-reanalysis.

In the following, we account for all referee comments in detail and include the track-change-version of the manuscript. **Remark:** We have not updated the responses that have been already published in gmdd (RC1, RC3). Hence, the referenced values therein differ from the final manuscript.

Authors' response

To gmd-2019-21 Anonymous Referee #1 (02 Apr 2019): We thank the referee for his/her useful comments and we will take them into account in the revised version of this paper. In the following, we will respond to the questions in detail.

- Abstract L15–17: *"While high sensitivity to changes in dry deposition to vegetation is found in the tropics, the largest impact on global scales is associated to changes in dry deposition to the ocean and deserts."* The authors do not provide details in the paper as to what has changed in the updated scheme for such an impact. We elaborate on the source of the *"largest impact on global scales"* in Section 3.2.2 (P18 L4–11). But we have to admit that it might not be clear to which resistance term the changes in the prescribed dry deposition velocities apply.

  - Is it the surface resistance (R_c) value? Or the other two resistances (R_a and R_b)? What are the typical values? It would be indeed interesting to look at the resistance terms separately. However, they are not available in our output files. Technically, it would be possible to force the model output but such would involve redoing the experiments and run for at least a couple of (model) weeks. In our formulation, the surface resistance R_c includes both stomatal and non-stomatal conductance. In case, of non-vegetated surfaces, such as *desert*, *ocean*, and *snow/ice*, the non-stomatal conductance, $G_{\mathrm{ns}}^{\mathrm{O_3}}$, is dominant. For water, $R_b = 10\,\mathrm{s\,m^{-1}}$ in most cases which is 2 orders of magnitude smaller than R_c. Thus, $R_{\mathrm{gs}}^{\mathrm{O_3}} \approx R_c^{\mathrm{O_3}} \propto (v_{\mathrm{DD}}^{\mathrm{O_3}})^{-1}$ (for R_c values see Table S2 in the manuscript Supplement S.3).
  - What value of R_c for water has been used and how it compares with the value used in the Wesely scheme? We have given the prescribed dry deposition velocities in Section 3.2.2:
    - For the *Wesely scheme* $v_{\mathrm{water}}^{\mathrm{O_3}} = 0.07\,\mathrm{cm\,s^{-1}}$ and
    - for the *EMEP scheme* $v_{\mathrm{water}}^{\mathrm{O_3}} = 0.05\,\mathrm{cm\,s^{-1}}$.

    Surface resistances for water are thus $R_c \approx 1429\,\mathrm{s\,m^{-1}}$ (*Wesely scheme*) and $R_c = 2000\,\mathrm{s\,m^{-1}}$ (*EMEP scheme*), respectively.

- P22 Table 3:

  - Why the deposition values for ocean + ice + land do to add up to the total values reported, for all simulations? Yes, that is, for we exclusively selected gridboxes associated to more then 98% to the three surface types (ocean, ice, and land), while *total* comprises all gridboxes. We admit that this is not clear. We shall repeat the computation of the values using the proper weighting and adapt the numbers (Table 5). We may also add that *ice* in this analysis only refers to regions at high latitudes that are permanently covered by ice and snow and hence does not take sea ice and mountain glaciers into account. In the Oslo CTM3, as written elsewhere in the manuscript, we compute dry deposition on ice and snow based on meteorological data. Therefore, the given values in Table 3 comprise ozone dry deposition on sea ice in the case of *ocean* and on snow covered land during winter in case of *land*.
  - The new land-based deposition values are much lower than what has been reported in previous studies (e.g. Hardacre et al., 2015) and the authors largely attribute this to the changes in the updated scheme for the desert surface type. However, the paper does not provide any observational support to back this up.
    - Are there any relevant deposition measurements (velocity or flux) that can be used for this purpose? Güsten et al. (1996) conducted measurements of ozone concentrations and fluxes onto the Sahara desert and deduced dry deposition velocities. We have not found any recent paper conducting field experiments in desert regions. We include a more thorough discussion of our results with respect to the observed fluxes by Güsten et al. (1996) and the references therein the revision of our manuscript.
    - At least, some comparison with ozone measurements (or even O_3 reanalyses) should be provided for this surface type (and perhaps others) to see if the model is heading in the right direction with the updated deposition scheme. Thank you for the advise. We will look into this.
  - It will also be useful to report the global ozone burden from the various simulations. Since Table 3 is already at maximum width with respect to the the page width, we shall show the global tropospheric ozone burden in a

Table 1. Total ozone dry deposition for the respective model experiment in $\mathrm{Tg\,a^{-1}}$. The global ozone dry deposition has been weighted by ocean, ice and, land fraction in each gridbox, respectively. *Ice* herein refers to regions at high latitudes that are permanently covered by ice and snow.

Experiment	Ocean			Ice			Land		
	NH	SH	Global	NH	SH	Global	NH	SH	Global
	($\mathrm{Tg\,a^{-1}}$)			($\mathrm{Tg\,a^{-1}}$)			($\mathrm{Tg\,a^{-1}}$)		
Wesely_type	159.7	147.8	307.5	3.6	6.3	9.9	446.6	193.7	640.3
EMEP_full	107.6	105.2	212.8	2.5	5.5	8.0	296.6	135.0	431.6
EMEP_offLight	110.0	105.8	215.8	2.5	5.4	7.9	337.1	156.0	493.0
EMEP_offPhen	108.0	105.3	213.2	2.5	5.5	8.0	301.6	139.1	440.7
EMEP_SWVL4	109.2	107.0	216.2	2.6	5.5	8.1	303.6	138.2	441.8
EMEP_ppgs	107.6	105.2	212.7	2.5	5.5	8.0	299.5	135.3	434.9
EMEP_ppgssh	108.3	105.4	213.6	2.5	5.5	8.0	306.8	142.8	449.6
EMEP_ppgssh_ice	107.4	105.3	212.7	1.2	1.6	2.8	303.0	144.1	447.2
EMEP_ppgs_2005	106.9	103.5	210.4	2.6	5.4	8.0	297.9	131.8	429.7

separate table (see the following Table 6). If we compare our results with Stevenson et al. (2006) ($344 \pm 39\,\mathrm{Tg}$) and the number given in IPPC AR5 (2013) ($337 \pm 23\,\mathrm{Tg}$), we find that the ozone burden in the Oslo CTM3 is higher then the model average from the start (*Wesely scheme*). The implementation of the *EMEP scheme* increases the tropospheric burden by roughly 8 % (compare *Wesely type* and EMEP_full).

Table 2. Annual mean tropospheric ozone burden for all experiments and 1σ standard deviation.

Experiment	Trop. O_3 (Tg)		
Wesely type	361	$\pm$	21
EMEP_full	392	$\pm$	28
EMEP_offLight	388	$\pm$	26
EMEP_offPhen	392	$\pm$	27
EMEP_SWVL4	402	$\pm$	31
EMEP_ppgs	392	$\pm$	28
EMEP_ppgssh	391	$\pm$	27
EMEP_ppgssh_ice	403	$\pm$	31
EMEP_ppgs_2005	386	$\pm$	26

– Section 2.1.1, Eq. (2): The statement *"For certain values of z, z0, and L, this may result in nonphysical (negative) values for Ra."* I do not comprehend as to why this would occur since this equation is simply based on the well-used Monin-Obukhov similarity theory (MOST) for the surface layer. This occurrence would also imply negative wind speeds. Actually Eq. (2) is incorrect: the term $\psi_m((z-d)/z_0)$ should be $\psi_m((z-d)/L)$, and the sign of the third term on the right-hand side should be positive (not negative). Given that $(z-d) > z_0$ (assuming the model is formulated correctly), Eq. (2) should always yield positive values.
Eqs. (3–5): I am not sure why Monteith (1973) needs to be invoked here. Given that the term in the square brackets on right hand side of Eq. (2) is equal to $k \cdot u(z)/u^*$ as per MOST, substituting this into Eq. (2) results in Eq. (5). Define z, z_0 in Eq. (2). The parameter d is the so-called displacement height, and is not a constant (depends on the surface type). The reviewer is indeed correct that this equation is wrong. In fact, we originally used Eq. (2) with L in the denominator for the second term. The sign error was likely the reason why the *Monteith method* was chosen. Certainly, an update shall be considered in the future, but it is not feasible to redo all simulations now. In the revised version of the manuscript, we change the text from *"In Simpson et al. (2003,2012) it is described as [...] fall back to the [...]"* to *"For technical reasons, we have used the [...]"*.

- P2 L25-33: The first reference to the Oslo CTM3 in the body of the paper is made here as *"...we have not implemented any parameterization of these processes in the Oslo CTM3 as of now."*
  - Some brief introductory text is required here (or better at the start of the paragraph) to introduce the model properly. The Oslo CTM3 is properly introduced in Section 2. Hence, we move the sentence in L30-32 about *polar boundary layer ozone depletion* to Section 2: *"Although the ozone depleting events in the polar boundary layer (Section 1) are important to understand surface ozone abundance in Arctic regions in spring-time, no parameterization of these processes is implemented in the Oslo CTM3 as of now."*
  - Also, the text between lines 25 – 33 on what is not considered in the model is too detailed to be here, so shorten and move it to Section 2. Given that the influence of VSLS on tropospheric ozone is indirect (through depletion of ozone in the upper troposphere – lower stratosphere and subsequent STE), this reference (L32–33) rather belongs to the discussion in Section 4 and will be moved: *"In particular, the STE depends on the stratospheric ozone abundance which is, e.g. affected by very short-lived ozone depleting substances (VSLS) (Warwick et al., 2006; Ziska et al., 2013; Hossaini et al., 2016; Falk et al., 2017) and is not taken into account in the Oslo CTM3."*

- P3 L19/L28 and P21 L34: There is a newer ozone dry deposition study by Luhar et al. (2018, ACP, 18, 4329-4348) which, using global ozone reanalyses and a more realistic process-based oceanic deposition scheme, estimates the total global deposition at $722.8 \pm 87.3\,\mathrm{Tg O_3 yr^{-1}}$, which includes an oceanic component of $98.4 \pm 30.0\,\mathrm{Tg O_3 yr^{-1}}$. These figures should be cited for comparison. Thank you for pointing this out. We were not aware of this study and will compare our results and refer to it at the given places and within our discussion.
  - *"A newer study by Luhar et al. (2018), however, indicates much lower amounts* ($722.8 \pm 87.3\,\mathrm{Tg\,a^{-1}}$)."
  - *"Based on the global atmospheric composition reanalysis performed in the ECWMF project Monitoring Atmospheric Composition and Climate (MACC) and a more realistic process-based oceanic deposition scheme, Luhar et al. (2018) found that the ozone dry deposition to oceans amounts to* $98.4 \pm 30.0\,\mathrm{Tg\,a^{-1}}$."
  - *"But also the results of Luhar et al. (2017, 2018) yield a* $(19-27)\,\%$ *lower ozone dry deposition than the models participating in the model intercomparison, with deposition to ocean ranging between* $(12-21)\,\%$ *of the total annual ozone dry deposition."*

- P11 Section 2.2: Since the present paper is about ozone dry deposition, this section seems like a distraction and hence should be omitted. The referee is right in his/her assessment. We therefore omit this section in the revised version of our manuscript.

- P14 L15-18: Anthropogenic, biomass burning, and biogenic emissions are included in the model. How are other emissions such as soil $\mathrm{NO_x}$, wetland methane, and oceanic methane and CO specified? Emissions from soil and wetlands are computed by MEGAN. Resultant $\mathrm{NO_x}$ emissions are upscaled to match Global Emissions InitiAtive (GEIA) inventory. For oceanic emissions of CO, we use predefined global fields (POET, available through ACCENT/GEIA, http://accent.aero.jussieu.fr/database_table_inventories.php). $\mathrm{CH_4}$ is taken from surface data from the EU project Hydrogen, Methane and Nitrous oxide: Trend variability, budgets and interactions with the biosphere (HYMN; EU GOCE 037048) for the year 2003 and scaled to oceanic amounts of $\mathrm{CH_4}$ from NASA (https://www.esrl.noaa.gov/gmd/ccgg/trends_ch4/) given for the years 2000–2004. We shall include this information in the revised manuscript.

- P15 L4: The statement *"Accidentally, we have used emissions for the year 2014 instead of 2005."* It is not clear what the consequences on the results are of this? In the introduction to Section 3.1, we wrote *"For all model integrations, the meteorological reference year is 2005. This choice only affects the comparison with data and multi-model studies that either perform analysis on decadal averages or differing years."*. We will clarify the sentence with respect to probable consequences.

- Section 3.2.1:

- Section 3.2.1: In the Fig 5 discussion, although snow and ice is discussed, there is no discussion on the oceanic differences between the present study and Hardacre et al. (2015). This is particularly important for the Southern latitudes. We agree that ozone dry deposition to oceans is of high importance for the southern hemisphere, last but not least in the zonal band $(50-70)^{\circ}\mathrm{S}$. In fact, we have mainly discussed out results with respect to seasonal cycles of dry deposition velocities onto ocean found in Hardacre et al. (2015) (Fig. 7; P21 L1–10: *"Similarly, the dry deposition velocities over water differ. [...]"*). We will include a discussion based on Fig. 5 in the revision of the manuscript.
- The Hardacre et al. (2015) simulations were for the year 2001, whereas the present study is mostly for the year 2015 emissions (see Table 1) driven by the year 2005 meteorology. In addition, the observational averages used in Fig. 8 are based on multi-year data. The authors should discuss the implications of these differences about different years on the deposition results presented (e.g. uncertainty). We regard this remark as a follow-up of the question raised regarding P15 L4. We will elaborate on the discussion regarding the implications based on our model results (EMEP_ppgs vs EMEP_ppgs_2005) in the revision of the manuscript. Though, the major consequence of this is that, for the majority of our model experiments, one can neither directly compare to observations for the years 2005 and 2014 nor to other the model results. Emission inventories may always be lacking in certain chemical species and the non-linearities in ozone formation and destruction make ozone concentrations sensitive to both emissions of precursors and meteorological conditions. Surface ozone observations, in fact, show a strong variability in ozone dry deposition and ozone concentrations at the sites. But studying these in detail may be well beyond the scope of this manuscript.

- P24 L3–4: *"The annual amount of ozone dry deposition decreases by up to 100% changing from the old dry deposition scheme to the new one."* Table 3 does not support this, but this may be true for some surface types. So please qualify the statement. We have indeed not specified our statement in the mentioned sentence, while we had done so elsewhere in the manuscript (P15 L12). We complete our statement in the revised version of the manuscript: *"[...] ozone dry deposition decreases by up to* $100\,\%$ *over all major desert areas [...]. At the same time, it increases over tropical forest.*

- P24 L15: *"Most of the decrease in ozone dry deposition in the Oslo CTM3 can be attributed to changes in dry deposition velocities over the ocean and deserts."* What are the dominant factors in these changes? For example, is it mostly the surface resistance (R_c) term? For the ocean, it is likely to be R_c. For deserts, maybe R_b? Is it possible to quantify these differences in the resistance terms? We have already answered the question with respect to ocean (see first bullet point). In summary, since R_b is quite small in most of the cases, the dominant factor for the ozone dry deposition onto ocean is the surface resistance R_c which is tabulated in Table S2. Regarding ozone dry deposition onto deserts, we use Eqs. (7–8) to deduce

$$R_b^i = \frac{2}{\kappa u_*} \cdot \left(\frac{D_{\mathrm{H_2O}}}{D_i} \cdot \frac{\mathrm{Sc_{H_2O}}}{\mathrm{Pr}} \right)^{\frac{2}{3}}, \tag{1}$$

with $\mathrm{Pr} = 0.72$, $\kappa = 0.4$, $\mathrm{Sc_{H_2O}} = 0.6$, $D_{\mathrm{H_2O}}/D_i = 1.6$. We estimate u_* from Eq. (16.67) in Seinfeld and Pandis (2006)

$$u_*(h) = \frac{\kappa \cdot \overline{u_x}(h)}{\ln(h/z_0)}, \tag{2}$$

with $h = 8\,\mathrm{m}$, $z_0^{\mathrm{desert}} \approx 10^{-3}\,\mathrm{m}$, and wind speeds not exceeding a gentle breeze ($1.8\,\mathrm{km\,h^{-1}} \leq \overline{u_x}(h) \leq 28\,\mathrm{km\,h^{-1}}$), we find $272\,\mathrm{s\,m^{-1}} \geq R_b \geq 17\,\mathrm{s\,m^{-1}}$. This is $1-2$ orders of magnitude smaller than $R_c = 2000\,\mathrm{s\,m^{-1}}$ and thus not negligible for low wind speeds. In summary, R_c is dominant in our formulation of dry deposition of ozone to deserts (unless we have calm wind conditions).

- P24 L24: *"2-layer gas exchange with ocean waters (Luhar et al., 2017)."* As mentioned earlier, Luhar et al. (2018) has derived a more realistic process-based deposition scheme for the ocean, but the results for deposition velocity do not seem to be too different from those in Luhar et al. (2017). We acknowledge Luhar et al. (2018) an update the sentence: *"[...] 2-layer gas exchange with ocean waters (Luhar et al., 2017, 2018)."*

– P25 L11–12: The comment *"This is most likely reflecting the ongoing industrialization process of countries in the southern hemisphere and the commitment and implementation of air quality regulations of industrialized nations in the northern hemisphere"* is quite speculative and may be omitted. We follow the kind advise of the referee and remove the sentence in the revised version of the manuscript.

– Eq. (13) cf. Eq. (14): g_{STO} or G_{sto} – use consistency with notation. Thanks for pointing this out. We will change this in the revised version of the manuscript.

– The first half of the abstract, the text before *"In this paper...,"* is introductory material and can be deleted. This is indeed the case and we will remove it in the revised version.

– Abstract L15–16: it is better to say "...leading to an increase in surface ozone of up to 100% in some regions." We follow the advice of the referee and change the sentence accordingly.

– P22 L7: *"At about 4 of 6 sites."* About? Not sure? Thanks for pointing out the misplaced *"about"* in this sentence. We are certain regarding that number.

Authors' response

To gmd-2019-21 referee#2 David Simpson (10 Apr 2019): We apologize for the confusion the misuse of the terms *EMEP* and *EMEP scheme* may have caused. We evaluated the major concerns raised in the review and found them severe enough that we have to revise our model and repeat the model experiments to address all concerns. Nevertheless, we will respond to all of the questions and concerns in more detail in the following.

Major points

- Mosaic formulation:
  - CTM3 claims to implement a mosaic approach, but instead of calculating deposition rates over each land-cover, and then aggregating using Eqn.3, CTM3 seems to perform the following steps:

$$R_a = \frac{u_z}{u_*^2} \tag{3}$$

$$\overline{Gs_g^i(z)} = \Sigma_{k=1}^{N} f_k \times Gs_{g,k}^i(z) \tag{4}$$

$$\overline{Gns_g^i(z)} = \Sigma_{k=1}^{N} f_k \times Gns_{g,k}^i(z) \tag{5}$$

As far as I can tell from the text, R_a is calculated once, with the same value of u_* for all land-covers. The CTM3 R_b calculation seems to also use the same u_* over different land-covers, except over sea where a more sophisticated scheme is used. Equations 2–3 above are equivalent to Eqns (22) and (26) from the manuscript. Now I am puzzled however as to how all this is put together. Do they use:

$$G_c = \mathrm{LAI} \cdot \overline{Gs_g^i(z)} + \overline{Gns_g^i(z)} \tag{6}$$

Thank you very much for your detailed account of the *mosaic approach*. It is correct that we use Eq. (4) and Eq. (5). As pointed out, we have not properly indicated the weighted mean in Eq. (22) and Eq. (29) in the manuscript. Additionally, there is also a typo in Eq. (13) and Eq. (22) (G_{sto} should have been g_{sto}). Eq. (22) should have read as follows:

$$\overline{g_{\mathrm{sto}}^{\mathrm{m}}} = \sum_{n=0}^{N} f_{\mathrm{L},n} \cdot g_{\mathrm{sto},n}^{\mathrm{m}} \tag{7}$$

All is put together in Eq. (13):

$$G_c = \mathrm{LAI} \cdot \overline{g_{\mathrm{sto}}^{\mathrm{m}}} + \overline{G_{\mathrm{ns}}} \tag{8}$$

We acknowledge that Eq. (13) should not proceed the other equations and that this might have caused additional confusion.

  - In any case, I think this approach has serious problems. Why average first for G_s and then for G_{ns} , when it is the fluxes (F_k , or $V_{g,k}^i(z_{\mathrm{ref}}) \times \chi_{\mathrm{avg}}^i(z_{\mathrm{ref}})$) which need to be averaged? I also do not understand why they would use the same u_* and R_a for all land-covers. I think the authors need to make a case for their approach, or change it. We have discussed the concerns raised and found that we have indeed made a mistake in our implementation of the *mosaic approach* which forces us to revise our model and repeat the model experiments. We update the equations in the revised manuscript accordingly.
- Calculation of R_a:

– R_a in CTM3 appears to be calculated just once, and from a height of 8 m. This means that there is no consistency between the R_a term and the underlying surface, which is clearly wrong. The similarity equation for R_a given in their Eqn (2) is very standard and has been used for decades (Garratt 1992). As pointed out by Ref 1, the equation as given has errors. Eq. (2) in our manuscript is indeed erroneous. The correct equation is (e.g., Erisman, 1994):

$$R_a = \frac{1}{\kappa u_*}\left[\ln\left(\frac{z-d}{z_0}\right) - \Psi_m\left(\frac{z-d}{L}\right) + \Psi_m\left(\frac{z_0}{L}\right)\right]. \tag{9}$$

– The correct equation will not give negative values unless presented with wrong inputs, and I suspect that that is what has happened. It is actually difficult to tell what was tested from the manuscript though, since they state simply that d is 'typically 0.7 m'. Did they use d properly, consistent with the underlying land-cover and its z_0? Did they assume that their 8 m meteorology was at a physical height of 8 m, or at $d + 8\,\mathrm{m}$. If the latter, which d? At that point, it is indeed neither clear from the manuscript nor from our internal documentation. The assumption that Eq. (2) (in the manuscript) would become negative, was most likely based on a wrong form of the integrated stability function Ψ_m.

Given $z = z_{\mathrm{ref}} = 8\,\mathrm{m}$ and $d = 0.7 \cdot 1\,\mathrm{m}$, it is right that neither the correct Eq. (9) nor the erroneous equation will result in negative R_a. The statement "d is 'typically 0.7 m'" is incorrect, indeed. We correct: *"[...]* $d_k = 0.78 \cdot h_k(\mathrm{lat})$, $z_0^k = 0.07 \cdot h_k(\mathrm{lat})$ *for forests,* $d_k = 0.7 \cdot h_k(\mathrm{lat})$, $z_0^k = 0.1 \cdot h_k(\mathrm{lat})$ *for vegetation other than forests [...]".* Side note: The average height of the lowermost model level is actually $20\,\mathrm{m}$ ($10\,\mathrm{m}$ for mid-level).

– Lines 19–30 of this section explain the Monteith alternative, but in a rather confusing way. For example, when is z_0 ever zero, as stated on line 23, or why does $\partial_z R_a \to R_a$ for finite z? (I know what they intend to say, but it isn't at all clear.) The referee is right. The text and derivation of the Monteith relation is confusing and also erroneous. In a revised version of the dry deposition scheme, we do no longer use these formulations, hence they are removed from the revised manuscript. Nevertheless, the correct form should have read as follows:

$$\Phi_{Q_{\text{sensible}}} = \rho_{\text{air}}\, c_P \cdot \frac{\Delta T}{R_{a,H}}. \tag{10}$$

$$\Phi_{Q_{\text{sensible}}} = \rho_{\text{air}}\, c_P \cdot \frac{\partial T}{\partial u} \cdot u_*^2. \tag{11}$$

For finite z, $\partial T \to \Delta T$.

– In any case, here the authors end up with a stability-independent equation for R_a, without mentioning or discussing that fact. In the revision of the model, we are going to implement the stability dependent R_a following Eq. (9) and update the manuscript accordingly.

– This very shallow layer is also very problematic for deposition calculations in general, since the model cell seems to be run here with horizontal dimensions of $2.25 \times 2.25°$, or about $250 \times 250\,\mathrm{km}$ near the equator, but a vertical mid-level (CTM3's z_{ref}) of just 8 m. Now, profiles of wind and depositing gases are very sensitive to the underlying surface, and should be very different for forests or lakes for example. Any wind-speed or friction velocity calculated from a model of such large horizontal resolution will necessarily give values at 8 m which reflect the whole grid. Deposition rates for a specific land-cover will vary enormously depending on what else is in the grid-square. (Although not strictly comparable, we showed in Schwede et al. (2018) that differences between the grid-average and forest specific deposition rates of N-compounds could be as much as a factor of two and up to more than a factor of five in extreme cases. These differences were largely dependent on how much forest occupied each grid cell.) Thank you for pointing this out. Indeed, an evaluation of winds at $8\,\mathrm{m}$ does not make much sense, given that forests in the tropics reach heights up to $40\,\mathrm{m}$. In S2012, R_a is actually evaluated "at around $45\,\mathrm{m}$" which is similar to the center of our second lowest model level. We correct for this in the revised model version.

- Why so much focus on sea areas?: The text seems rather unbalanced with regard to the different land-covers. Sect. 2 uses 1/2 page on various z_0 corrections for oceans, but say nothing about the ecosystem where ozone is expected to deposit at high rates: forests, crops, and other terrestrial ecosystems. The supplementary has three Figs related to this oceanic deposition. Why? The referee is right that ozone is predominately deposited to terrestrial ecosystems, which cover about 2/9 of the Earth's surface, while 2/3 is covered by oceans. Nevertheless, due to the ocean's vastness, relatively small changes in modeled dry deposition easily accumulate and influence the atmospheric ozone concentration as pointed out in Hardacre et al. (2015) based on Ganzeveld et al. (2009). Luhar et al. (2017, 2018) show that the current models may overestimate the oceanic ozone sink by a factor of three – rendering the ocean a even smaller sink for ozone.

  This said, Section 2 as a whole consists of about 9 pages, of which 1/2 page is dedicated to oceans (R_b computation) and 7 pages are dedicated to vegetation especially stomatal and non-stomatal conductance (R_c computation). Hence, we do not see a significant unbalance in favor of oceans herein.

  Regarding the three figures with respect to ocean in the supplementary material: The reason for these is that we found some "legacy code" in the model (linear fit to dynamic viscosity of air $\mu(T)$) after we had finished the implementation of the new dry deposition scheme, run the experiments, and done the analysis on these. We had to verify that this had no significant influence on the results.

- Use of the term 'EMEP scheme'?: Sect. 3 discusses the comparisons of V_g in terms of 'EMEP scheme' versus 'Wesely scheme', and sensitivity tests are named e.g. 'EMEP_offlight'. As noted above the scheme implemented in CTM3 is very different to that implemented in the EMEP model, so this is very misleading. Please rename your scheme to something else. I am worried that readers might get the impression that it is the EMEP scheme which is being tested here, but it certainly is not. [...] We apologize for the misleading naming of the new dry deposition scheme in the Oslo CTM3 which is (partly) based on the formulations in the publication the referee refers to as *S2012*. By no means have we meant to offend any of the original authors of the EMEP/MSC-W model nor intended to misguide the readers. We will rename the revised scheme appropriately (→*mOSaic scheme*).

- Reproduction of material from S2012:

  - As far as I can see, Table S1, S2 and S3 are taken directly from S2012, with no change to parameters. It is not usual to copy tables from the work of other authors in this way. Just refer to S2012 (and give Table number as help). We will follow this advice and refer to the tables in S2012 accordingly.
  - Many of the equations are from S2012, and many not. I would like the authors to make this very explicit, so that readers are not confused as to what comes from EMEP, and what has changed for CTM3. We are going to elaborate on this matter in a revised version and refer to our equations' sources more properly.

Minor points

- P1 L22. Isn't H_2O the most important greenhouse gas? (Say anthropogenic GHG perhaps?) Thank you for pointing this out. We follow the advice and write: *"[...] ozone is a potent anthropogenic greenhouse gas [...]"*

- P2 L3. The Wilson ref only concerns Europe, and its focus on the 95th percentile can hide trends found at higher percentiles (e.g. Simpson et al. 2014). A better ref would be Fleming et al. (2018) or Mills et al. (2018a). By the way, the most recent calculation on food security (using flux approaches) is now Mills et al. (2018b).

  Thank you for pointing out these publications. We take them into consideration, when revising the manuscript.

- P2 L11. What does in situ mean here? Ozone production can take place over days of transport. *In situ* typically means *on site, locally*. In this context, we used it exactly in this meaning. We elaborate on this in a revised version of the paper: *Elevated ozone levels at a site may originate from both, the local production of ozone from its precursors, which are transported, and from advection of ozone itself. Long-range ozone transport occurs regularly and might be most important in regions that else lack precursors. Tropospheric ozone is produced in complex photochemical cycles involving precursor gases [...]*

- P2 L25–35. This text about halogens is not really relevant to a dry deposition paper. Reactions with bromine can be important sinks, but are not usually counted as deposition. The removal of ozone from the Arctic boundary layer in the presence of halogens is indeed not part of ozone dry deposition and we remove this reference in this context. Although these processes are not relevant with respect to ozone dry deposition, they matter regarding the observed ozone abundances in the Arctics. One of the proposed mechanisms to trigger bromine explosions involves, e.g., an "initialization" by ozone dry deposition.

- P3 L2–3. Why specify mid-June maximum for ozone. Monks (2000) might take issue with that, as would for example Sinha et al. (2015). The referee has got a point here. Of cause the maximum of ozone in the annual cycle depends on the location. We remove this specification.

- P3 L4–5. There are plenty of ozone measurements made outside Europe. The authors appear to be unaware of the massive ozone collections made under the TOAR project (see e.g. Flemming, Mills refs below), or the high quality data available from GAW (inha 2015). Thank you for reminding us of the data collected under the TOAR project. We knew about this data set but have to admit that we have not made much use of it, yet. We have, however, not stated that there are, in general, no sites outside of Europe, but that long-term observations (started before the 1950s) are only found in Europe. Maybe the term "long-term" is not clear enough. We add: *"From the observational side, the number of long-term observations (started before the 1950s) is limited and restricted to mainly European sides."*

- P3 L16. One also has dry deposition to water, as this paper makes clear later on. That is indeed true, but we didn't want to name all possible surfaces onto which dry deposition takes place. We, hence, shall write: *"Removal of any substance from the atmosphere which is not involving rain, e.g., through gravitational settling or by uptake by plants, soil, and water, is referred to as dry deposition.*

- P3 L20. One usually refers to dry deposition as something between a near- surface height (e.g. z = 1m, 10m, or 50m) and the surface, not from z_0. In fact, at $z = z_0$ one has $u_z = 0$, and hence the author's R_a just below should be zero. Thank you for pointing out this inaccuracy. We, of cause, meant "near-surface" height or lowermost model level (which is indeed not at $z_0 = 0$). We change the text accordingly: *"[...] dry deposition is a product between near-surface ozone concentration* $[\mathrm{O_3}](\mathrm{z_0})$ *(e.g. the lowermost model level) [...] "*

- P4 L20. I would remove the term textbook knowledge, since there are many different approaches to nearly all these equations. It is thus good that the equations as used in CTM3 are spelled out explicitly. We follow the advice and remove the sentence in which the term occurs and write: *"[...] we will give a detailed account of the new dry deposition scheme and the equations that we use."*

- P5 L5. I would add Emberson et al. (2000a) and Tuovinen et al. (2004) to the list of EMEP refs here, since this was the first publication of the methods that have more or less been used until today. We have added the references regarding the EMEP MSC-W model. *"[...] we mainly follow Simpson et al. (2012) in their description of dry deposition used in the European Monitoring and Evaluation Programme (EMEP) MSC-W model (see also, Emberson et al., 2000; Simpson et al., 2003; Tuovinen et al., 2004;), [...]"*

- P7, notation. In S2012 and EMEP generally, we use upper-case G and R to refer to canopy-scale (bulk) variables, and lower-case for leaf-scale. Thus, in EMEP we would have $G_{\mathrm{sto}} = LAIg_{\mathrm{sto}}$. Here the authors seem to mix upper and lower case between their equations (13) and (14). We have indeed mixed up the cases here.

- P7 Eqn (13). Is LAI one-sided, 2-sided, projected .... define. LAI is one-sided taken from ISLSCP2 FASIR. We add this to the sentence: *"[...] LAI is the one-sided leaf area index taken from ISLSCP2 FASIR [...]"*

- P8 L1. S2012 do not suggest using depths lower than 1 m. We use SMI3 which is from 28-100 cm. Thank you for the clarification. This may have been a misunderstanding on our side. Since we have to repeat our simulations, we will choose the appropriate SWVL from the start.

– P8 L2. Why did you choose to use the surface (0–7 cm) soil moisture? Initially we choose 0–7 cm due to the original scope of this work within our research project, in which we study ozone concentrations and uptake by plants in boreal regions where the soil columns are expected to be more shallow then, e.g., at mid-latitudes. We expect the stomatal conductance in these environments to be more sensitive to precipitation. Using the actual water availability to vegetation, would be better, but this is not feasible without a proper land surface model.

– P8 L18. This is wrong. Nothing in the EMEP model is used to 'mimic the time lag..'. We use the light function to modify stomatal conductance, as with the other f factors. We change this inadequate formulation: *"[...] this integrated photon flux is used to modify the stomatal conductance in response to light."*

– P9 L20, and Table 1. The consequence of Table 1 is that vegetation at $0.5^\circ\,\mathrm{N}$ will start growing at day 90, whereas those at $0.5^\circ\,\mathrm{S}$ will start on day 272. (By the way, in EMEP now we use monthly factors from the LPJ-GUESS model to derive phenology for non-European areas, because of such difficulties with tabulations.) Thank you for the remark. We see this problem. Using an actual land model would solve this, but at that point it is not feasible to integrate such in the Oslo CTM3.

– P9 L18. What do you mean by "surface or 2 m"? Surface might refer to skin or leaf temperature? This may have been indeed unclear. It is the $2\,\mathrm{m}$ temperature. We change the text accordingly: *"[...] $\theta_{2\mathrm{m}}$ is the $2\,\mathrm{m}$ temperature in $^\circ\mathrm{C}$."*

– P9 Eqn (26). Say 1st and 2nd, not I. and II. We follow the advise regarding Eq. (26) and also change Table 1 accordingly.

– P9 Eqn (27). This equation is a modification of Erisman's original (1994) formulation, so explain that. We follow the advise and write: *"The in-canopy resistance R_{inc} (Erisman et al., 1994) is then modified with respect to each (vegetated) land type N [...]"* We have added the respective reference in the text.

– P10 L12. Be explicit that this statement refers to S2012. The current EMEP model uses different heights for e.g. tropical vegetation. We follow this advice and write: *"The vegetation height $h(N, lat)$ as described by Simpson et al. (2012) [...]"*

– P11 Sect 2.2. I also found this aerosol section confusing. Eqn (30) is from S2012, and so is the factor 0.008.SAI/10 used in Eqn (33), but here new a_1 coefficients are defined. Did the 'aerosol microphysic model' referred to also mix equations in this way? Is there any publication as to the reliability of this method? The a_1 coefficients were calculated from deposition velocities taken from the Oslo CTM2 (Oslo CTM2 list of publications, online). We meant to use this new scheme for aerosols in the Oslo CTM3, but as of now it has not been evaluated and is actually not used. Hence, we will remove this section from the paper and add: *"In addition to the gaseous species, Simpson at al. (2012) also modify aerosol deposition velocities, namely black carbon (BC) and organic carbon (OC), sulfuric aerosols ($\mathrm{SO_4}$, MSA) and secondary organic aerosols (SOA), but we have not updated our model with respect to these."*.

– P12 Fig.2. I didn't understand what is being done here. The Figure suggests that the EMEP scheme has one category for 'Forests, Med. scrub', whereas S2012 lists 4 types of forest, as well as Mediterranean scrub as a separate ecosystem. This figure also suggests that EMEP has savanna, which it doesn't, but do have many other categories (Table 3 of S2012 lists 16 main categories. The current EMEP model has 32.) The caption may become clearer after we changed the name of our scheme, so that it can no longer be confused with the actual EMEP model. The purpose of the mapping is to project the more detailed categories for stomatal conductance to the ground-surface resistance categories (Table S19 in S2012 supplement). We have updated figure and text in accordance to the corrections made in the model code. It should be clearer now.

– P12 L13. Again, the current EMEP model is not eurocentric, and uses global phenology calculations. We follow the advice and drop the term "eurocentric" the text: *"Since the parameterization of SGS and EGS in Simpson et al. (2012) is not applicable [...]"*

– P13 Sect 2.3.2. The initial lines (14-16) are hard to understand and only by reading further do I see what they mean by 'de-accumulated'. If working with IFS PPFD is so hard, why didn't the authors just calculate hourly (or minute-by- minute)

PPFD using cloud-cover and zenith angles? We elaborate on the comprehensibility of this paragraph: *"From OpenIFS an accumulated surface PAR is available. It is integrated both, spectral (presumably* $400 - 60\,\mathrm{nm}$*) and temporally. For practical use in Eq. (18), we de-accumulate this field with respect to time and refer to the result as PPFD."* We have not used that ansatz, because we do not have the radiation fields in the relevant wavelengths available from OpenIFS output.

Authors' response

To gmd-2019-21 Anonymous Referee #1 (01 May 2019): We thank the referee for his comments. Taking all comments from both referees into consideration, we find it necessary to revise our model and redo the simulations.

– The authors state in their response that *"In fact, we originally used Eq. (2) with L in the denominator for the second term. The sign error was likely the reason why the Monteith method was chosen. Certainly, an update shall be considered in the future, but it is not feasible to redo all simulations now."* The fact of the matter is that there have been some fundamental inconsistencies in the formulation of this equation, and the authors' logic of "it is not feasible to redo all simulations now" is not tenable. Ideally, the simulation would need to be done again. At the very least, the authors need to perform some test runs which demonstrate whether or not the inconsistencies in Eq. (2) make any significant difference to the results. The authors have also not clarified how the value of the zero-plane displacement height d is selected. They simply state that d is constant (typically 0.7m). Looking up any atmospheric boundary-layer text book (e.g. Garratt, 1992), d is approximately 0.7 times the canopy height (or the height of the roughness element). Please check this for consistency too. We will address all matters for which we have to repeat the simulations, e.g., calculation of R_a , output of dry deposition velocities, etc., at the same time. We will also check the definition of the replacement height d in our formulation.

Update and evaluation of the ozone dry deposition in the Oslo CTM3 v1.0

Stefanie Falk[1] and Amund Søvde Haslerud[2,a]

[1]Department of Geosciences, University of Oslo, Oslo, Norway
[2]CICERO Center for International Climate Research, Oslo, Norway
[a]Kjeller Vindteknikk, Kjeller, Norway

Correspondence: Stefanie Falk (stefanie.falk@geo.uio.no)

Abstract. High concentrations of ozone in ambient air are hazardous not only to humans but to the ecosystem in general. The impact of ozone damage on vegetation and agricultural plants in combination with advancing climate change may affect food security in the future. While the future scenarios in themselves are uncertain, there are limiting factors constraining the accuracy of surface ozone modeling also at present: The distribution and amount of ozone precursors and ozone depleting substances, the stratosphere-troposphere exchange as well as scavenging processes. Removal of any substance through gravitational settling or by uptake by plants and soil is referred to as dry deposition. The process of dry deposition is important for predicting surface ozone concentrations and understanding the observed amount and increase of tropospheric background ozone. The conceptual dry deposition velocities are calculated following a resistance-analogous approach wherein aerodynamic, quasi laminar, and canopy resistances are key components, but these are hard to measure explicitly. ~~In this paper, we~~ We present an update of the dry deposition scheme implemented in the Oslo CTM3. We change from a purely empirical dry deposition parameterization to a more process-based one which is taking the state of the atmosphere and vegetation into account. ~~Examining~~ We examine the sensitivity of the scheme to various parameters, ~~our focus lies mainly on~~ e.g. the stomatal conductance-based description of the canopy resistance ~~. We~~ and the choice of ozone surface resistance, and evaluate the resulting modeled ozone dry deposition with respect to observations and multi-model studies~~and~~ . Individual dry deposition velocities are now available for each land surface type and agree generally well with observations. We also estimate the impact on the modeled ozone concentrations at the surface. We show that the global annual total ozone dry deposition decreases with respect to the previous model version (~~−47 %~~−37 %), leading to an increase in surface ozone of ~~up to~~ more than 100 % in some regions. While high sensitivity to changes in dry deposition to vegetation is found in the tropics and the northern hemisphere, the largest impact on global scales is associated to ~~changes in dry deposition to~~ the choice of prescribed ozone surface resistance the ocean and deserts.

1 Introduction

Ozone is an important trace gas for all lifeforms on Earth. Depending on the place of its occurrence it has either a positive or negative connotation. In the stratosphere, ozone absorbs most of the ultraviolet (UV)-light from the sun within the range of 100–315 nm, thus shielding the Earth's surface from the most harmful UV-radiation. In addition, ozone is a potent greenhouse gas in both, stratosphere and troposphere. With a radiative forcing of $0.40 \pm 0.20\,\mathrm{W\,m^{-2}}$, it is placed third, only surpassed by

CO_2 and CH_4 (IPCC - Intergovernmental Panel on Climate Change, 2013, Chapter 8).

In the troposphere and in particular in ambient air, ozone is considered as a highly toxic pollutant. Since the industrial revolution, tropospheric background ozone concentrations have been increasing in the northern hemisphere (IPCC - Intergovernmental Panel on Climate Change, 2013, Chapter 2). In recent years, the number of episodes of peak concentrations has been, in general, decreasing in North America and Europe due to the implementation of air quality regulations ~~(e.g., Wilson et al., 2012)~~ (e.g., Fleming et al., 2018; Mills et al., 2018). At the same time, fast developing countries, like e.g., China or India, saw a significant increase in ozone related air pollution. Continuously high concentrations of ambient air ozone are hazardous to the whole ecosystem. It is estimated that ozone is cause to an increase in pre-mature deaths (WHO - World Health Organization, 2008), an average global loss of yield in the four major crops (wheat, rice, maize, and soybean) of about $3-15\,\%$ (Ainsworth, 2017) as well as $7\,\%$ loss in primary production in forestry (Wittig et al., 2009; Matyssek et al., 2012). The impact of ozone damage on vegetation and agricultural plants may affect food security in the future especially in Asia ~~(Tang et al., 2013; Tai et al., 2014; Chuwah et al., 2015)~~ (Tang et al., 2013; Tai et al., 2014; Chuwah et al., 2015; Mills et al., 2018) and might be an important additional feedback to climate change (Sitch et al., 2007).

Elevated ozone levels at a site may originate from both, the local production of ozone from its precursors, which are transported, and from advection of ozone itself. Long-range ozone transport occurs regularly and might be most important in regions that else lack precursors. Tropospheric ozone is ~~mainly produced in situ in~~ produced in complex photochemical cycles involving precursor gases such as carbon monoxide (CO) or volatile organic substances (VOCs – also known as hydrocarbons) in the presents of nitrogen oxides (NO_x). A typical reaction mechanism for CO is sketched in the following. In a sequence of rapid reactions a peroxyl radical $HO_2^\bullet$ is formed through an initial reaction of CO with a hydroxyl radical $^\bullet OH$. Via a reaction between $HO_2^\bullet$ and NO, NO_2 is formed which is then photolyzed. The resulting atomic oxygen reacts then with O_2 (and also under the presence of available co-reactants) to form an ozone molecule. Such a cycle leads to a net production via:

$$CO + 2O_2 + h\nu \rightarrow CO_2 + O_3. \tag{R1}$$

Similar cycles involving VOCs exist (Monks et al., 2015). Another source of tropospheric ozone is downward transport from the stratosphere via stratosphere-troposphere exchange (STE) (WMO - Global Ozone Research and Monitoring Project, 2014). Based on observations, STE might only amount to ~~roughly~~ $10\,\%$ ($550 \pm 140\,\mathrm{Tg\,a^{-1}}$) of the total global ozone budget in the troposphere, while ozone from chemical production is estimated to be $5000\,\mathrm{Tg\,a^{-1}}$ (Monks et al., 2015). Ozone is removed from the atmosphere by photochemical reactions or scavenging processes. Major sinks are photolysis followed by a reaction with water vapor to from OH, reactions with HO_2, titration reactions, and dry deposition. We will come back to the latter later in this section and cover the implemented scheme in more detail in Section 2.1.

~~A dry deposition related sink limited to Arctic regions are so called ozone depleting events. They occur in spring-time in the polar boundary layer where an outburst of bromine monoxide (so called bromine explosion) leads to a rapid depletion of surface ozone (Oltmans, 1981; Bottenheim et al., 1986; Barrie et al., 1988; Bottenheim and Chan, 2006). Various schemes ranging from bulk-snow parameterization (Toyota et al., 2011; Falk and Sinnhuber, 2018) to detailed in-snow (Toyota et al., 2014) , and aerosol chemistry (Yang et al., 2010) have been successfully applied to different types of atmospheric models but do not~~

yet cover the full range of observed events. Although these ozone depleting events are important to understand surface ozone abundance in Arctic regions, we have not implemented any parameterization of these processes in the Oslo CTM3 as of now. We also do not consider the contribution of very short-lived ozone depleting substances (VSLS), that affect stratospheric ozone (Warwick et al., 2006; Ziska et al., 2013; Hossaini et al., 2016; Falk et al., 2017), to the tropospheric ozone abundance.Since ozone is highly reactive, its global mean life-time in the troposphere is roughly 22 days but ranges between a few days in the tropical boundary layer to up to 1 year in the upper troposphere (Stevenson et al., 2005; Young et al., 2013). The abundance of tropospheric ozone therefore varies, e.g., with time of the day(maximum ~15:00 local time), season(mid-June maximum), season, altitude, location (Schnell et al., 2015), or weather conditions in general (Otero et al., 2018). Typical concentrations of surface ozone range from $10\,\mathrm{ppb}$ over the tropical Pacific to $100\,\mathrm{ppb}$ in the downwind areas of highly emitting sources (IPCC - Intergovernmental Panel on Climate Change, 2013, Chapter 8). This variability poses a challenge on both, trend analysis from observation as well as validation and intercomparison of models. At From the observational side, there is only a limited the number of long-term ozone observations , mainly restricted to European sitesobservations (started before the 1950s) is limited and restricted to mainly European sides. Most of these indicate a doubling of tropospheric ozone since the 1950s (IPCC - Intergovernmental Panel on Climate Change, 2013, Chapter 2). But especially the very low pre-industrial ozone abundance cannot be reproduced by the likes of most models. Among the participating models in the Atmospheric Chemistry and Climate Model Intercomparison Project (ACCMIP), there is a general tendency to underestimate tropospheric ozone burden (e.g., $10-20\,\%$ negative bias at $250\,\mathrm{hPa}$ in the southern hemisphere (SH) tropical region) (IPCC - Intergovernmental Panel on Climate Change, 2013, Chapter 8). With respect to surface ozone, Schnell et al. (2015) conclude that all ACCMIP models, which reported hourly surface ozone, tend to overestimate surface ozone values in North America and Europe in comparison with available observations. A key to fathom these slightly contradicting results may lie in the used dry deposition schemes.

Removal of any substance from the atmosphere which is not involving rain, e.g., through gravitational settling or by uptake by plantsand soil, soil, and water, is referred to as dry deposition. The process of dry deposition is important for predicting surface ozone concentrations and understanding the observed amount and increase of tropospheric background ozone. It is estimated that about $1000 \pm 200\,\mathrm{Tg\,a^{-1}}$ of ozone are removed from the atmosphere by dry deposition processes (Monks et al., 2015). A newer study by Luhar et al. (2018), however, indicates much lower amounts ($722.8 \pm 87.3\,\mathrm{Tg\,a^{-1}}$). Conceptually, dry deposition is a product between surface near-surface ozone concentration $[\mathrm{O_3}](z_0)$ (e.g. the lowermost model level) and a dry deposition velocity $v_{\mathrm{DD}}^{\mathrm{O_3}}$. Species dependent dry deposition velocities v_{DD}^{i}, which are synonymously referred to as conductance G^i, for any gaseous species i, are typically calculated following a resistance-analogous approach

$$v_{\mathrm{DD}}^{i} = \frac{1}{R_a + R_b^i + R_c^i}, \tag{1}$$

wherein aerodynamic R_a, quasi-laminar layer R_b^i, and canopy resistances R_c^i are key components (Wesely, 1989; Seinfeld and Pandis, 2006). For all gases, R_a is the same, while R_b^i and R_c^i vary from gas to gas and also depend on land surface types (e.g., ice/snow, water, urban, desert, agricultural land, deciduous forest, coniferous forest etc.). Originally, Wesely (1989) used fixed seasonal average dry deposition resistances for each land surface type. For all three types of resistances in this Wesely-type parameterization, more process-oriented formulations have been developed and validated over the

years. Luhar et al. (2017) have validated ozone dry deposition to the ocean with respect to three different formulations of surface resistances. Based on the global atmospheric composition reanalysis performed in the ECWMF project Monitoring Atmospheric Composition and Climate (MACC) (MACC-II Consortium, 2011) and a more realistic process-based oceanic deposition scheme, Luhar et al. (2018) found that the ozone dry deposition to oceans amounts to $98.4 \pm 30.0\,\mathrm{Tg\,a^{-1}}$. An update on the ozone surface resistance over snow and ice covered surfaces has been provided from combined model and observation studies (Helmig et al., 2007, $v_{\mathrm{ice/snow}}^{\mathrm{O_3}} = 1/10000\,\mathrm{m\,s^{-1}}$). Canopy conductance is parameterized at the single-leaf-level (stomatal conductance) for various plant function types (PFT) as well as for single plant species based on empirical studies (Jarvis, 1976; Ball et al., 1987; Simpson et al., 2012; Mills et al., 2017). But progress has also been made on process-oriented modeling of stomatal conductance (Anderson et al., 2000; Buckley, 2017). The variety of differing formulations and choices of parameters leads to a wide spread of results in model intercomparisons (Hardacre et al., 2015; Derwent et al., 2018) and about $20\,\%$ uncertainty on the resulting total dry deposition (Monks et al., 2015).

In Section 2, we will briefly describe the Oslo CTM3, give a detailed account of the new dry deposition scheme (Section 2.1) as well as present pre-processing of meteorological input data to compute necessary input to the dry deposition scheme such as begin and duration of greening season (GDAY, GLEN) and photosynthetic photon flux density (PPFD) (Section 2.2). In Section 3, we present sensitivity tests with respect to a manifold of parameters in the dry deposition scheme (Section 3.1) and validate our results with respect to results from the multi-model intercomparison of Hardacre et al. (2015) (Section 3.2)~~and to observations at the surface~~ , the MACC-reanalysis (Section 3.3), and to surface ozone observations (Section 3.4). In Section 4, we will summarize and discuss our results and draw conclusions for further development of the model.

2 Model description

The Oslo CTM3 is ~~a three dimensional~~an offline, three dimensional, global chemistry transport model (CTM). The key components of the Oslo CTM3 have been described and evaluated by Søvde et al. (2012). A detailed account of the capabilities of the Oslo CTM3 in simulating anthropogenic aerosol forcing in the past and recent past using the Community Emission Data System (CEDS) historical emission inventory (Hoesly et al., 2018) is given by Lund et al. (2018). The Oslo CTM3 can also be coupled to the Model of Emissions of Gases and Aerosols from Nature (MEGAN v2.10) (Guenther et al., 2006). A publication focusing on this is planed.

While the meteorological data driving the Oslo CTM3 is given in a resolution of T159N80L60, with the highest model level at $0.02\,\mathrm{hPa}$, it is very time and memory consuming to run the Oslo CTM3 with full chemistry at this resolution. Therefore, we reduced the horizontal resolution to $2.25^\circ \times 2.25^\circ$ in our experiments. In the following, we will give a detailed account of the new dry deposition scheme ~~. Although some of the equations in this section may be *textbook knowledge*, for the sake of completeness, it is important to summarize them, nonetheless~~and the equations that we use.

2.1 Ozone dry deposition scheme

In the original dry deposition scheme~~of the Oslo CTM3~~, the state of the atmosphere was not taken into account. Dry deposition velocities were rather parameterized following the work of Wesely (1989) with parameter updates from Hough (1991). This means that seasonal day and night average deposition velocities for different land surface types (water, forest, grass, tundra/desert, and ice and snow) were in use. Day was distinguished from night by solar zenith angles below $90\,^{\circ}$. Winter was defined by temperatures below $273.15\,\mathrm{K}$ for gridboxes containing land masses. For ocean, winter and summer parameters are equal in this parameterization, therefore no distinctive treatment ~~is~~ was needed for ocean gridboxes. In addition, a reduced uptake due to snow cover above $1\,\mathrm{m}$ for forest and $10\,\mathrm{cm}$ for grass/tundra, respectively, was taken into account. We will refer to this parameterization as *Wesely scheme*.

Regarding the new dry deposition scheme, we ~~follow~~ mainly follow Simpson et al. (2012) in their description of dry deposition used in the European Monitoring and Evaluation Programme (EMEP) MSC-W model ~~(Simpson et al., 2003, 2012)~~(see also, Emberson et a , which is used for air quality modeling implementing the Convention on Long-Range Transboundary Air Pollution (CLRTAP). We will refer to ~~this as~~ the new scheme as ~~*EMEP*~~ *mOSaic scheme* throughout the rest of the paper. The ~~EMEP~~ mOSaic scheme is a more physical approach compared to the previously used Wesely scheme, because it takes state (e.g., pressure, temperature) of the atmosphere as well as dynamics (e.g., wind stress) of the boundary layer into account. To a certain degree, the global variety of plants and their variability throughout the seasons is also acknowledged. The ~~EMEP~~ mOSaic scheme is implemented for the gaseous species O_3, H_2O_2, NO_2, PAN, SO_2, NH_3, HCHO, and CH_3CHO. Since CO has a very small uptake and is not included in Simpson et al. (2003, 2012), the Wesely parameterization is kept. In addition to the gaseous species, ~~some of the~~ Simpson et al. (2012) also modify aerosol deposition velocities~~are also modified~~, namely black carbon (BC) and organic carbon (OC), sulfuric aerosols (SO_4, MSA) and secondary organic aerosols (SOA), but we have not updated our model with respect to these.

As displayed in Eq. (1), the dry deposition computation is ~~typically split into three different resistance contributions (aerodynamic R_a,quasi-laminar layer R_b^i, and canopy R_c^i) which we will recap in the following.~~ subdivided into contributions from three different resistances. The main idea of a mosaic approach is to calculate these resistances separately for each land surface type k in each grid cell: R_a^k,$R_b^{i,k}$, and $R_c^{i,k}$. The grid cell average dry deposition velocity $\overline{v}_{\mathrm{DD}}^i$ is then defined by weighting each individual $v_{\mathrm{DD}}^{i,k}$ by the corresponding land fraction factor f_k:

$$\overline{v}_{\mathrm{DD}}^i = \sum_k f_k v_{\mathrm{DD}}^{i,k} \tag{2}$$

2.1.1 Aerodynamic resistance

~~The aerodynamic resistance is describing~~ In general, the aerodynamic resistance describes the turbulent transport of any substance down to the surface. ~~In Simpson et al. (2003, 2012) it is described as~~ To derive R_a^k, we follow Simpson et al. (2003, 2012)

and compute a local friction velocity at reference height z_{ref} (Eq. (52), Simpson et al., 2012)

$$R_a u_*^k = \frac{1}{\kappa u_*} \ln\left(\frac{z-d}{z_0}\right) - \Psi_m \frac{z-d}{z_0} - \Psi_m \frac{z_0}{L} \frac{\overline{u}(z_{\mathrm{ref}}) \cdot \kappa}{\ln\left(\frac{z_{\mathrm{ref}}-d_k}{z_0^k}\right) - \Psi_m\left(\frac{z_{\mathrm{ref}}-d_k}{L}\right) + \Psi_m\left(\frac{z_0^k}{L}\right)}, \tag{3}$$

with the average wind speed $\overline{u}(z_{\mathrm{ref}})$ at reference height, the Kármán constant $\kappa = 0.40$, the ~~friction velocity u_*, integrated stability equations~~ integrated stability equation for momentum Ψ_m ~~, a constant d (typically $0.7\,\mathrm{m}$), and the~~ (e.g., Garratt, 1992) , a grid average Obukhov length L. ~~For certain values of z, z_0, and L, this may result in nonphysical (negative) values for R_a. For this reason, we diverge from the EMEP scheme at this point and fall back to the method of Monteith (1973), wherein~~ , deplacement height d_k, and roughness length z_0^k ($d_k = 0.78 \cdot h_k(\mathrm{lat})$, $z_0^k = 0.07 \cdot h_k(\mathrm{lat})$ for forests, $d_k = 0.7 \cdot h_k(\mathrm{lat})$, $z_0^k = 0.1 \cdot h_k(\mathrm{lat})$ for vegetation other than forests). Taking the height of vegetation in to consideration, we have chosen the model level such that $\overline{z}_{\mathrm{ref}} \approx 45\,\mathrm{m}$. Using the derived u_*^k from Eq. (3), a local Obukhov length L_k can be obtained from (Eq. (8), Simpson et al., 2012):

$$L_k = -\frac{\rho c_p T_{2\mathrm{m}} u_*^k}{\kappa g H}. \tag{4}$$

Herein, H is the sensible heat flux ~~$\Phi_{Q_{\mathrm{sensible}}}$ is written as~~

$$\Phi_{Q_{\mathrm{sensible}}} = \rho_{\mathrm{air}}\, c_P \cdot \frac{\partial_z T}{\partial_z R_a}.$$

~~Herein, ρ_{air} is the air density, c_P~~ , g is the standard gravitational acceleration, c_p the specific heat ~~at constant pressure P, $\partial_z R_a$ is the diffusion resistance to sensible heat between surface ($z_0 = 0$) and the reference height z, and $\partial_z T$ is the difference between the surface temperature T_0 and the temperature at a reference height T_z. From the eddy diffusion theorem, a similar formulation can be derived~~

$$\Phi_{Q_{\mathrm{sensible}}} = \rho_{\mathrm{air}}\, c_P \cdot \frac{\partial_z T}{\partial_z u} \cdot u_*^2.$$

~~Comparing Eq. (10) and Eq. (11) and assuming $\partial_z R_a \to R_a$ and $\partial_z u \to u_z$ for a finite z, we find~~

$$R_a = \frac{u_z}{u_*^2}.$$

~~As reference height z, we use the height at mid-level of the lowermost model level (roughly $8\,\mathrm{m}$). From the meteorological input fields u_z is directly available, while u_* can be computed via~~

$$u_* = \sqrt{\frac{\tau_0}{\rho}},$$

~~with the turbulent surface stress $\tau_0^2 = \mathrm{NSSS}^2 + \mathrm{EWSS}^2$, and northward turbulent surface stress (NSSS), eastward turbulent surface stress (EWSS)~~ capacity, and T_{2m} the $2\,\mathrm{m}$ temperature. With these, we can compute the aerodynamical resistance for each land surface type (Eq. (8.8), Simpson et al., 2003)

$$R_a^k = ..., \tag{5}$$

with the integrated stability equation for heat Ψ_h (e.g., Garratt, 1992). Both integrated stability functions (Ψ_m, Ψ_h) and corresponding parameters are listed in supplement S.1.

2.1.2 Quasi-laminar layer resistance

The quasi-laminar layer resistance ~~R_b^i~~ $R_b^{i,k}$ is species specific and differs over land and ocean surfaces. ~~In case a gridbox contains both, a weighted mean is calculated.~~ Over land, we use (Eq. (53), Simpson et al., 2012)

$$R_b^{i,k} = \frac{2}{\kappa u_*} \cdot \left(\frac{\mathrm{Sc}_i}{\mathrm{Pr}}\right)^{\frac{2}{3}}, \tag{6}$$

wherein Pr is the Prandtl number (~~typically~~ 0.72 for air and other gases) and Sc_i is the Schmidt number for a gas i. Eq. (6) differs from a similar formulation in Seinfeld and Pandis (2006) by a factor of roughly 1.25. From $\mathrm{Sc}_i = \nu / D_i$, with the kinematic viscosity of air ν, we derive a Schmidt number in water equivalent:

$$\mathrm{Sc}_i = \frac{D_{\mathrm{H_2O}}}{D_i} \cdot \mathrm{Sc}_{\mathrm{H_2O}}, \tag{7}$$

with the molecular diffusivity for any gas D_i, the Schmidt number of water ($\mathrm{Sc}_{\mathrm{H_2O}} = 0.6$) and its molecular diffusivity ($D_{\mathrm{H_2O}} = 0.21 \cdot 10^{-4}\,\mathrm{m^2\,s^{-1}}$). The used ratios $D_{\mathrm{H_2O}}/D_i$ are ~~tabulated in Supplement S.1.~~ taken from Simpson et al. (2012, Table S18).

Over ocean, we use (Eq. (54), Simpson et al., 2012)

$$R_b^i = \frac{1}{\kappa u_*} \cdot \ln\left(\frac{z_0}{D_i} \cdot \kappa u_*\right) \tag{8}$$

with an imposed lower threshold of $10\,\mathrm{s\,m^{-1}}$ and an upper limit of $1000\,\mathrm{s\,m^{-1}}$. The computation of roughness length z_0 over ocean is divided into a *calm* and a *rough* sea case, with a threshold of $3\,\mathrm{m\,s^{-1}}$. For calm sea, we apply the following upper limit (Hinze, 1975; Garratt, 1992, with a slightly higher coefficient of 0.135)

$$z_0^{\mathrm{calm}} = \min\left\{2 \cdot 10^{-3}, 0.135 \cdot \frac{\nu}{u_*}\right\}. \tag{9}$$

The kinematic viscosity of air ν herein can be computed from

$$\nu = \frac{\mu}{\rho} = \frac{\mu(T)}{\frac{P_0}{T \cdot R_{\mathrm{air}}}}. \tag{10}$$

For the temperature dependent dynamic viscosity of air $\mu(T)$, we chose a linear fit to Sutherland's law through the origin within the temperature range $\{T \in \mathbb{R} | (243.15 < T < 313.15)\,\mathrm{K}\}$: $\mu(T) = 6.2 \cdot 10^{-8}\,\mathrm{kg\,m^{-1}\,s^{-1}\,K^{-1}} \cdot T$. But despite its rough accuracy, we found that the choice of $\mu(T)$ has no effect on ~~$\overline{R_b}$~~ $\overline{R}_b^{i,k}$ (Supplement S.2: Figs. S1–S2). In Eq. (10), ρ is substituted by the air density using the ideal gas law. P_0 is the surface pressure, as T the 2 m temperature is chosen, and R_{air} is the universal gas constant for air. The rough sea case follows the method of Charnock (1955); Wu (1980):

$$z_0^{\mathrm{rough}} = \min\left\{2 \cdot 10^{-3}, 0.018 \cdot \frac{u_*^2}{g}\right\} \tag{11}$$

with a gravitational acceleration $g = 9.836\,\mathrm{m\,s^{-2}}$. The allowed maximum roughness length in both cases is set to $2\,\mathrm{mm}$. Since the z_0 computed with this parameterization are rather small ($0 < z_0^{\mathrm{calm}} < 1 \cdot 10^{-4}\,\mathrm{m}$, $0 < z_0^{\mathrm{rough}} < 2 \cdot 10^{-3}\,\mathrm{m}$), R_b^i is set to its lower limit of $10\,\mathrm{s\,m^{-1}}$ in about $91\,\%$ of all cases (see Supplement S.2: Fig. S3).

2.1.3 Surface resistance

The surface resistance consists of both, stomatal and non-stomatal resistances. ~~When computing gridbox averages, we use the sum of conductances (deposition velocities)~~

$$G_c = \mathrm{LAI} \cdot G_{\mathrm{sto}} + G_{\mathrm{ns}},$$

~~wherein LAI is the leaf area index (zero for non-vegetated surfaces), G_{sto} the stomatal conductance, and G_{ns} the non-stomatal conductance.~~

The stomatal conductance is a measure of the rate of CO_2 exchange and evapotranspiration through the stomata of a leaf. There are several environmental conditions affecting the opening and closing of the stomata and hence ~~their~~ the capability of respiration (e.g., light, available water, etc.). Stomata sluggishness, a state in which the stomata can no longer fully close, has been reported as ozone induced damage (Hoshika et al., 2015), but is not taken into account in our formulation. To reflect part of the underlying mechanism, the ~~stomatal conductance g_{STO} in the EMAP~~ leaf-level stomatal conductance in the mOSaic scheme is computed using a ~~multiplicative ansatz that is also explained in much detail in Mills et al. (2017)~~common multiplicative ansatz (Ball et al., 1987; Mills et al., 2017):

$$g_{\mathrm{STO}}^{k}{}_{\mathrm{sto,\,m}} = g_{\mathrm{max}}^{\mathrm{m}}{}_{\mathrm{max,\,m}}^{k} \cdot f^{k}{}_{\mathrm{phen}} \cdot f^{k}{}_{\mathrm{light}} \cdot \max\{f_{\mathrm{min}}, f_T \cdot f_D \cdot f_{\mathrm{SW}}\} \max\left\{f_{\mathrm{min}}^k, f_T^k \cdot f_D^k \cdot f_{\mathrm{SW}}^k\right\}. \tag{12}$$

The factors herein are normalized and vary within the range $0-1$. They account for leaf phenology (f_{phen}), light (f_{light}), temperature (f_T), water vapor pressure deficit (f_D), and soil water content (f_{SW}). All factors differ with land use type k. For clarity reasons, we drop this index in the following, as long as it is not necessary for the equation's completeness.

The temperature adjustment f_T ~~of plants~~ is computed from

$$f_T = \frac{T_{2\mathrm{m}} - T_{\mathrm{min}}}{T_{\mathrm{opt}} - T_{\mathrm{min}}} \cdot \left(\frac{T_{\mathrm{max}} - T_{2\mathrm{m}}}{T_{\mathrm{max}} - T_{\mathrm{opt}}}\right)^{\beta}, \tag{13}$$

with $\beta = \frac{T_{\mathrm{max}} - T_{\mathrm{opt}}}{T_{\mathrm{opt}} - T_{\mathrm{min}}}$. The parameters T_{min}, T_{max} and T_{opt} are tabulated for various ~~land surface~~ plant functional types. All parameters ~~used in the EMEP scheme can be found in the supplementary to Simpson et al. (2012) or tabulated in Supplement S.3~~are taken from Simpson et al. (2012, Tables S16, S19). Since f_T turns negative outside ~~its~~ the range defined by T_{min}, T_{max}, we impose a lower limit of 0.01 for numerical reasons.

The water vapor deficit (VPD) is proportional to the saturation partial pressure of water ($P^s_{\mathrm{H_2O}}$) and relative humidity (RH)

$$\mathrm{VPD} = P^s_{\mathrm{H_2O}} \cdot (1 - \mathrm{RH}/100). \tag{14}$$

Using tabulated values of f_{min}, D_{min}, D_{max}, the water vapor pressure deficit penalty factor f_D can be computed:

$$f_D = f_{\mathrm{min}} + (1 - f_{\mathrm{min}}) \cdot \frac{D_{\mathrm{min}} - \mathrm{VPD}}{D_{\mathrm{min}} - D_{\mathrm{max}}}. \tag{15}$$

The penalty factor with respect to available soil water (SW) f_{SW} is defined as

$$f_{\mathrm{SW}} = \begin{cases} 1 & \textit{if} \quad \mathrm{SW} \geq 0.5, \\ 2 \cdot \mathrm{SW} & \textit{if} \quad \mathrm{SW} < 0.5. \end{cases} \tag{16}$$

~~Simpson et al. (2012) suggest using SW of soil depths below 1 m (SWVL4 in OpenIFS). Throughout most of our simulations (Section 3), we have, however, used the soil water contained in the top layer (SWVL1, $0-7\,\mathrm{cm}$), which makes the canopy conductance more sensitive to precipitation than it would be otherwise~~SW is evaluated at a soil depths of $0.28-1\,\mathrm{m}$, which corresponds to SWVL3 in OpenIFS.

The phenology of a plant typically describes its life-cycle throughout a year, e.g., at mid latitudes and for deciduous species, it starts with the emergence of leafs in spring and ends in fall. In the ~~EMEP~~ mOSaic scheme, phenology is parameterized with respect to the start of ~~the~~ greening season (SGS) and its end (EGS). Details about our treatment of these are given in Section 2.2.1. In summary, our adaption of the f_{phen} parameterization reads as follows:

$$f_{\mathrm{phen}} = \begin{cases} \textit{if} \quad \mathrm{GLEN} \geq 365 & 1 \quad \textit{(explicitly excluding tropics)} \\ \textit{if} \quad \mathrm{GDAY} = 0 & 0 \\ \textit{else} & \begin{cases} \textit{if} \quad \mathrm{GDAY} \leq \phi_{\mathrm{AS}} & \phi_a \\ \textit{if} \quad \mathrm{GDAY} \leq \phi_{\mathrm{AS}} + \phi_e & \phi_b + (\phi_c - \phi_b) \cdot (\mathrm{GDAY} - \phi_{\mathrm{AS}})/\phi_e \\ \textit{if} \quad \mathrm{GDAY} \leq \mathrm{GLEN} - \phi_{\mathrm{AE}} - \phi_f & \phi_c \\ \textit{if} \quad \mathrm{GDAY} \leq \mathrm{GLEN} - \phi_{\mathrm{AE}} & \phi_d + (\phi_c - \phi_d) \cdot (\mathrm{GLEN} - \phi_{\mathrm{AE}} - \mathrm{GDAY})/\phi_f \\ \textit{else} & \phi_d \end{cases} \end{cases} \tag{17}$$

Herein, we use the SGS and EGS derived parameters day of greening season (GDAY), the time elapsed starting at the SGS, and the total length of the greening season (GLEN), the time span between EGS and SGS. The parameters ϕ_a, ϕ_b, ϕ_c, and ϕ_d define start or end points in the five phases of phenology in the ~~EMEP~~ mOSaic scheme, while ϕ_e, ϕ_f, ϕ_{AS}, and ϕ_{AE} control the temporal timing (Fig. 1). If GLEN is zero we are, e.g., in Arctic regions and there is no vegetation anyway, therefore $f_{\mathrm{phen}} = 0$. Before the start of the ~~growing~~ greening season ($\mathrm{GDAY} = 0$) $f_{\mathrm{phen}} = 0$. Since ~~the EMEP scheme~~ this phenology is tuned to northern hemisphere (NH) mid latitudes, ~~this phenology~~ it does not apply to the tropics~~, after evaluation of the model results (Section 3.1), we~~. We therefore decided to set $f_{\mathrm{phen}} = 1$ if GLEN is greater or equal to 365 which is the case in the tropics.

Light in the wavelength band $400-700\,\mathrm{nm}$ to which the plant chlorophyll is sensitive is called photosynthetic active radiation (PAR). The integral of PAR over these wavelengths is the photosynthetic photon flux density (PPFD). ~~In the EMEP parameterization, this integrated photon flux is used to mimic the time lag of the opening and closing of stomata with respect to light instead of a simple day-on/night-off treatment~~The correction factor f_{light} in response to varying PPFD is:

$$f_{\mathrm{light}} = 1 - \exp(-\alpha_{\mathrm{light}} \cdot \mathrm{PPFD}). \tag{18}$$

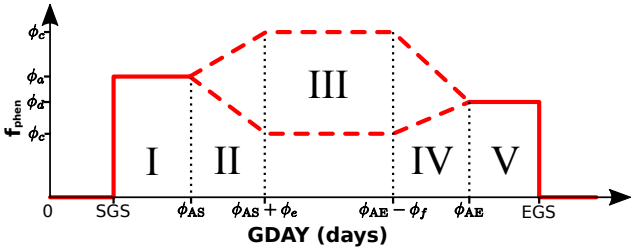

Figure 1. Sketch of the five different phases in plant phenology f_{phen} in accordance to Eq. (17).

Since ~~g_{max}~~ $g_{\text{max, m}}$ in Eq. (12) is in units of $\mathrm{mmol\,s^{-1}\,m^{-2}}$, a unit conversion ~~is done:~~ to $\mathrm{m\,s^{-1}}$ is necessary in our model:

$$g^{\mathrm{m}\,k}_{\text{sto}}(N) = g_{\text{sto}}(N)^{k}_{\text{sto, m}} \cdot R \cdot \frac{T_0}{P_0}. \tag{19}$$

Herein, R is the universal gas constant. ~~With these, the total gridbox stomatal conductance G_{sto} is computed weighted by the land surface type fraction $f_L(N)$:~~

$$G_{\text{sto}} = \sum_{N=0}^{N_{\text{max}}} f_L(N) \cdot g^{\mathrm{m}}_{\text{sto}}(N)$$

In the ~~EMEP~~ mOSaic scheme, non-stomatal conductances are explicitly calculated for O_3, SO_2, HNO_3, and NH_3. For all other species, an interpolation between O_3 and SO_2 values is carried out.

The non-stomatal conductance for O_3 consists of two terms, one depending on vegetation type and one depending on the soil/surface. For ~~a land surface type N~~ each land surface types k, we can write

$$G_{\text{ns}}{}^{\mathrm{O_3}}(N)^{\mathrm{O_3},k} = \frac{\mathrm{SAI}(N)}{r_{\text{ext}}}\frac{\mathrm{SAI}_k}{r_{\text{ext}}} + \frac{1}{R_{\text{inc}}(N) + R^{\mathrm{O_3}}_{\text{gs}}(N)}\frac{1}{R^{k}_{\text{inc}} + R^{\mathrm{O_3},k}_{\text{gs}}}. \tag{20}$$

~~$\mathrm{SAI}(N)$~~ SAI_k is the surface area index for vegetation type ~~N~~k, which is LAI plus ~~some value representing~~ a value that represents cuticles and others surfaces. The external leaf resistance is defined by

$$r_{\text{ext}} = 2000\,\mathrm{s\,m^{-1}} \cdot F_T. \tag{21}$$

Herein F_T is a temperature correction factor for temperatures below $-1\,^{\circ}\mathrm{C}$ and $\{F_T \in \mathbb{R} | (1 \leq F_T \leq 2)\}$

$$F_T = \exp(-0.2 \cdot (1 + \theta_0))\exp(-0.2 \cdot (1 + \theta_{2\mathrm{m}})). \tag{22}$$

Table 3. Definition of growing season for crops used in the Oslo CTM3 in northern hemisphere (NH) and southern hemisphere (SH).

	~~I.~~ 1st part (days)	~~II.~~ 2nd part (days)
NH	90–140	141–270
SH	272–322	323–452

~~θ_0 is the surface or~~ $\theta_{2\mathrm{m}}$ is the $2\,\mathrm{m}$ temperature in $^\circ\mathrm{C}$. ~~In general,~~ For most land surface types, $\mathrm{SAI} \equiv \mathrm{LAI}$~~for all land types, except for~~. Some exceptions are:

$$\mathrm{SAI} = \begin{cases} \mathrm{LAI} + 1 & \textit{if} \quad \textit{forest / wetland}, \\ \mathrm{LAI} \cdot 5/3.5 & \textit{if} \quad \textit{cropland}, \text{ 1st part of growing season}, \\ \mathrm{LAI} + 1.5 & \textit{if} \quad \textit{cropland}, \text{ 2nd part of growing season}, \\ 0 & \textit{if} \quad \textit{cropland}, \text{ winter}. \end{cases} \tag{23}$$

Extending the ~~EMEP~~ mOSaic scheme to the southern hemisphere, ~~the used~~ we use the growing season for crops ~~is~~ defined in Table 3.

In this way, vegetation affects the conductance also by being there, not only by uptake through the stomata. The in-canopy resistance R_{inc} ~~is defined for each vegetated land type N as~~ (Erisman et al., 1994) is then modified with respect to each (vegetated) land surface type in k

$$R_{\mathrm{inc}} = b \cdot \mathrm{SAI}(N)_k \cdot \frac{h(N,\mathrm{lat})}{u_*} \frac{h_k(\mathrm{lat})}{u_*}, \tag{24}$$

where ~~$h(N,\mathrm{lat})$~~ $h_k(\mathrm{lat})$ is the latitude dependent vegetation height (see explanation at the end of this section) and ~~$b = 14\,\mathrm{s}^{-1}$~~ $b = 14\,\mathrm{m}^{-1}$ is an empirical constant. ~~According to Simpson et al. (2012), the canopy resistance in EMEP~~ The canopy resistance described in Simpson et al. (2012) does not take temperature and snow into account and is zero for non-vegetated surfaces, but we will adopt the correction previously used in the Oslo CTM3 Wesely scheme.

~~$R_{\mathrm{gs}}^{\mathrm{O_3}}(N)$ is tabulated and corrected for temperature by F_T and snow cover fraction f_{snow}:~~

$$\frac{1}{R_{\mathrm{gs}}^{\mathrm{O_3}}(N)} = \frac{1 - f_{\mathrm{snow}}}{\hat{R}_{\mathrm{gs}}^{\mathrm{O_3}}(N)} + \frac{f_{\mathrm{snow}}}{R_{\mathrm{snow}}^{\mathrm{O_3}}}.$$

As initially mentioned, the necessary depth of snow to cover a certain type of vegetation differs. Therefore, we calculate a snow cover fraction f_{snow} using the snow depth S_D, which is available in units of meter of water equivalent from the meteorological input data, scaled to $10\,\%$ of the vegetation height. $R_{\mathrm{gs}}^{\mathrm{O_3},k}$ is tabulated. We correct for temperature by F_T and for snow cover fraction:

$$\frac{1}{R_{\mathrm{gs}}^{\mathrm{O_3},k}} = \frac{1 - f_{\mathrm{snow}}^k}{\hat{R}_{\mathrm{gs}}^{\mathrm{O_3},k}} + \frac{f_{\mathrm{snow}}^k}{R_{\mathrm{snow}}^{\mathrm{O_3},k}}. \tag{25}$$

The ~~total conductance $G_{\mathrm{ns}}^{\mathrm{O_3}}$ in each gridbox is the sum of all $G_{\mathrm{ns}}^{\mathrm{O_3}}(N)$ weighted by the land surface type fraction $f_L(N)$~~

~~$$G_{\mathrm{ns}}^{\mathrm{O_3}} = \sum_{N=0}^{N_{\max}} G_{\mathrm{ns}}^{\mathrm{O_3}}(N) \cdot f_L(N).$$~~

bulk canopy conductance is then defined as:

$$G_c^k = \mathrm{LAI} \cdot g_{\mathrm{sto,\,m}}^k + G_{\mathrm{ns}}^k, \tag{26}$$

wherein LAI is the one-sided leaf area index taken from ISLSCP2 FASIR, g_{sto} the leaf-level stomatal conductance, and G_{ns} the bulk non-stomatal conductance.

2.1.4 Latitude dependent vegetation height

The vegetation height ~~$h(N,\mathrm{lat})$ in the EMEP scheme~~ $h_k(\mathrm{lat})$ as described by Simpson et al. (2012) is linearly decreasing with latitude between 60° and $74^\circ\mathrm{N}$. To adapt this to a global model, we ~~need to make~~ made a few additional assumptions. The tabulated height for each vegetation type ~~$h(N)$ in the EMEP~~ h_k in the mOSaic scheme is regarded as constant at mid latitudes ($40^\circ - 60^\circ$). Towards the poles, we decrease the height of each vegetation type using the same rate as described in Simpson et al. (2012). At a latitude of 74° a minimum height of ~~$3/10 \cdot h(N)$~~ $3/10 \cdot h_k$ is reached and kept constant. Towards the equator, we increase the height linearly so that at a latitude of 10° a maximum height of ~~$2 \cdot h(N)$ is achieved~~ $2 \cdot h_k$ is reached which is then held constant. We also assume symmetry in both hemispheres. Presuming a typical tree height of $20\,\mathrm{m}$ at mid latitudes, this step-wise function yields a height of $8\,\mathrm{m}$ at high latitudes and $40\,\mathrm{m}$ in the tropics which is not unrealistic. For four example PFTs, results are shown in the Supplement (S~~.4~~.3, Fig. S4).

2.1.5 Mapping of land surface types

The Oslo CTM3 is configured to read land surface types from, either ISLSCP2 product from MODIS or Community Land Model (CLM) 2 categories, which have to be mapped to the ~~nine~~ land surface types used in the ~~EMEP~~ mOSaic scheme (Fig. 2). For both, MODIS and CLM 2 land surface categories, snow and ice cover is estimated from input meteorology, while ~~water~~ f_L^{water} is defined as ~~$1 - \sum_{N=0}^{N_{\max}} f_L(N)$~~ $1 - \sum_k f_L^k$. From the MODIS category *Barren or sparsely vegetated*, everything polward from 60° is defined as tundra, while everything equatorward is categorized as desert. This mapping differs from the one used in the Wesely scheme.

2.2 ~~Dry deposition scheme for other gases and aerosols~~

~~For , , and , we follow exactly the treatment as described by Simpson et al. (2012). Since the dry deposition velocity for is very small, we use a prescribed value for $v_{\mathrm{DD}}^{\mathrm{CO}}$ of $0.03\,\mathrm{cm\,s^{-1}}$.~~

The EMEP scheme for aerosols (BC, OC, , , SOA) defines the surface deposition velocity V_{ds} as

$$\frac{V_{\mathrm{ds}}}{u_*} = \begin{cases} a_1 & \textit{if} \quad L \geq 0\,\mathrm{m}, \\ a_1 \cdot F_N \left[1 + \left(\frac{a_2}{25}\right)^{2/3}\right] & \textit{if} \quad -25\,\mathrm{m} < L < 0\,\mathrm{m}, \\ a_1 \cdot F_N \left[1 + \left(\frac{-a_2}{L}\right)^{2/3}\right] & \textit{if} \quad L \leq -25\,\mathrm{m}, \end{cases}$$

wherein $F_N = 3$ for fine nitrate and ammonium and $F_N = 1$ for all other species. L is again the Obukhov length. $a_2 = 300\,\mathrm{m}$, while a_1 differs for forest and non-forest. To account for hydrophilic and hydrophobic BC/OC aerosols on dry and wet surfaces, we diverge slightly from the EMAP scheme in the definition of the parameter a_1. From pre-studies with an aerosol microphysic model, we find

$$a_1^{\text{hydrophob.}} = 0.025\,\mathrm{cm\,s^{-1}} \cdot \overline{u_*}$$

and

$$a_1^{\text{hydrophil.}} = 0.2\,\mathrm{cm\,s^{-1}} \cdot \overline{u_*},$$

with the annual mean friction velocity $\overline{u_*}$. Our definition of a_1 is then:

$$a_1 = \ldots$$

The total aerosol surface deposition is defined as

$$V_{\mathrm{ds}}^{\mathrm{tot}} = \sum_{N=0}^{N_{\max}} V_{\mathrm{ds}}(N) \cdot f_L(N).$$

2.2 Pre-processing

As mentioned in the previous section, there are two variables needed for computing the stomatal conductance which are not directly available from the meteorological input data. The greening season, as the time of the year in the mid and high latitudes when it is most likely for plants to grow, and the photosynthetic photon flux density, as the amount of light that plants need to photosynthesize. In the following, we present the necessary pre-processing of the variables. It is planed to implement an online computation of these variables into the Oslo CTM3 later on.

2.2.1 Greening season

In Eqs. (20–23), Simpson et al. (2012) use prescribed start of growing season (SGS) and end of growing season (EGS) at $50\,^{\circ}\mathrm{N}$ (d_{SGS}, d_{EGS}) together with lapse rates (∇d_{SGS}, and ∇d_{EGS}) to define phenology and dry deposition over agricultural areas. For the growing season of crops in the computation of non-stomatal conductances, we use also prescribed values (Table 3), while

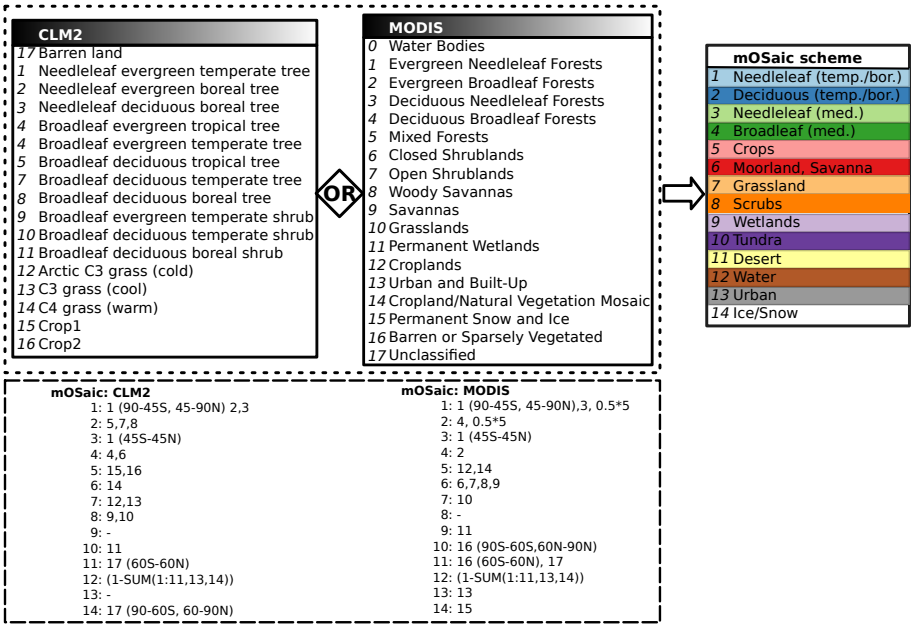

Figure 2. Mapping of land surface categories. Either land surface categories from ISLSCP2 product of MODIS ~~/~~ or the Community Land Model (CLM) 2 can be chosen for mapping to the ~~nine~~ land surface types ~~used~~ we use in the ~~EMAP~~ mOSaic scheme. Water bodies ~~and snow and ice categories~~ of MODIS are actually not mapped. For both, MODIS and CLM 2 land surface categories, snow and ice cover is estimated from input meteorology, while water is defined as ~~$1 - \sum_{N=0}^{N_{\max}} f_L(N)$~~ $1 - \sum_k f_L^k$. From MODIS category *Barren or sparsely vegetated*, everything polward from 60° is defined as tundra, while everything equatorward is categorized as desert.

for the stomatal conductances, as shown in Eq. (17), we use the SGS and EGS derived parameters: day of greening season (GDAY), the time elapsed starting at the SGS, and the total length of the greening season (GLEN), the time span between EGS and SGS. Since the ~~eurocentric EMEP~~ parameterization of SGS and EGS in Simpson et al. (2012) is not applicable in a global model, another latitude dependent parameterization is needed. First, we ~~have~~ used a parameterization ~~as~~ which was already implemented in the Oslo CTM3 and which had been adopted from the Sparse Matrix Operational Kernel Emissions – Biogenic Emission Inventory System (SMOKE-BEIS; model webpage). SMOKE-BEIS has fixed values for SGS and EGS for all regions but NH mid latitudes ($23^\circ < \text{lat} < 65^\circ$), where it uses lapse rates of $\nabla d_{\text{SGS}} = 4.5$ and $\nabla d_{\text{EGS}} = 3.3$. As this parameterization is optimized for North America, it does not work well in Europe, e.g., most of northern Scandinavia has no allocated vegetation period. This basically results in a suppression of canopy resistance in northern Scandinavia.

In agriculture, there are different empirical rules to estimate the SGS and EGS. The simplest assumption is that greening starts after 5 consecutive days with a daily average temperature above $5\,^\circ\text{C}$ and vice versa for EGS. Other estimates use growing degree days (Levis and Bonan, 2004; Fu et al., 2014a), include soil moisture (Fu et al., 2014b), or rely on satellite observations. A comprehensive evaluation of different techniques is given by Anav et al. (2017). Another solution would be the usage of a

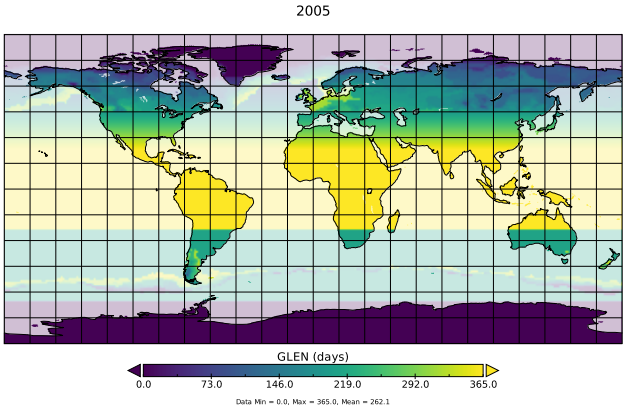

Figure 3. Pre-processing of greening season from meteorological surface temperature fields. Shown is the total length of the greening season (GLEN) for the year 2005. The $5\,^{\circ}$C-days criteria has been used in both hemispheres mid–high latitudes. Ocean has been shaded to indicate that greening season will only affect land.

proper land surface model, e.g. LPJ-GUESS, CLM, but the integration of such into the Oslo CTM3 is not planed at the moment.

Based on the empirical rule ($5\,^{\circ}$C-days), we have pre-processed our meteorological input data offline. We added some additional criteria to prevent for *false spring*: If, within these 5 days, the average temperature drops below or rises above $5\,^{\circ}$C, the counter is reset, respectively. First, we used the $5\,^{\circ}$C-days criteria for $45^{\circ} < \text{lat} < 85^{\circ}$ in the NH, but extended it also to $35^{\circ} < \text{lat} < 65^{\circ}$ in the SH. In all other cases and where the $5\,^{\circ}$C-days criteria fails, we still use the SMOKE-BEIS parameterization. The described algorithm written in python 2.7 has been included as Supplement S~~.5~~.4. An example map of the computed GLEN using the $5\,^{\circ}$C-days criteria in both hemispheres is shown in Fig. 3.

2.2.2 Photosynthetic photon flux density

From OpenIFS an accumulated surface PAR is available~~which is already integrated presumably over the spectrum~~. It is integrated both, spactrally (presumably $400 - 700\,\text{nm}$~~. For this reason, it will be refered to as PPFD instead of PAR. This PPFD field has not been de-accumulated in the post-processing of the OpenIFS output and it is not feasible to redo all of the post-processing for this work. But for~~) and temporally. For practical use in Eq. (18), ~~this field needs to be de-accumulated.~~ we de-accumulate this field with respect to time and refer to the result as PPFD.

The main obstacle is that PAR has been accumulated since model start, so that the first field kept from the original OpenIFS simulation ($00\,\text{UTC}$) is 12 hours after model start ($12\,\text{UTC}$ on the previous day). In other words, the first time step of each day in the Oslo CTM3 has already accumulated PAR from $12\,\text{UTC}$ on the previous day. De-accumulation of times $03\,\text{UTC}$ to $21\,\text{UTC}$, simply means computing the difference

$$\text{PPFD}(t_i) = \text{PAR}(t_{i+1}) - \text{PAR}(t_i). \tag{27}$$

For de-accumulation of the remaining ~~timestep~~time step, the best choice is subtracting the difference between 21 UTC and 12 UTC of the previous day

$$\mathrm{PPFD}(t = 00\,\mathrm{UTC}) = \mathrm{PAR}(t = 00\,\mathrm{UTC}) - [\mathrm{PAR}(t = 21\,\mathrm{UTC} - 1\,\mathrm{day}) - \mathrm{PAR}(t = 12\,\mathrm{UTC} - 1\,\mathrm{day})] \quad (28)$$

and limit the result to positive values only. An example PAR de-accumulation for January 2nd 2005 is shown in Supplement S~~.6~~.5 (Figs. S5–S7). The resulting PPFD fields are still accumulated over a time period of 3 hours and should be divided by 3. A known issue in the OpenIFS (cycles $\leq$ c41r2) causes surface PAR values to be about 30 % below observations. To counter this, we decided to refrain from the division at this stage, but need to bear this in mind for later OpenIFS cycles.

3 Evaluation

In this section, we present results from a manifold of Oslo CTM3 model integrations testing different parameters of the ~~EMEP~~ mOSaic scheme. We focus on changes in ozone ~~related to the stomatal conductance parameterization, e.g.,~~ total dry deposition $\sum \mathrm{O_3^{DD}}$, dry deposition velocities $v_{\mathrm{DD}}^{\mathrm{O_3}}$, ~~and surface concentration $[\mathrm{O_3}](z_0)$ or surface burden $\mathrm{O_3}(z_0)$ in units of , respectively~~concentrations in the lowermost model level $[\mathrm{O_3}](p_0)$, and tropospheric burden $\sum_{\mathrm{trop}} \mathrm{O_3}$. We evaluate our results with respect to the multi-model comparison of ozone dry deposition by Hardacre et al. (2015) (Section 3.2), the MACC-reanalysis (Section 3.3), and observations (Section 3.4). The Oslo CTM3 is driven by meteorological input fields from ECMWF – OpenIFS cy38r1. CEDS historical emission inventory is used for anthropogenic emissions, while biomass burning is covered in daily resolution by NASA's Global Fire Emissions Database, Version4 (GFEDv4). Biogenic emissions are taken from MEGAN-MACC output (Sindelarova et al., 2014), while emissions from soil and wetlands are computed by MEGAN. Resultant $\mathrm{NO_x}$ emissions are up-scaled to match Global Emissions InitiAtive (GEIA) inventory. For oceanic emissions of CO, we use predefined global fields from POET (GEIA-ACCENT emission data portal, 2003). Emissions of $\mathrm{CH_4}$ are taken from the EU project (EU GOCE 037048) Hydrogen, Methane and Nitrous oxide: Trend variability, budgets and interactions with the biosphere (HYMN) for the year 2003 and scaled to oceanic amounts of $\mathrm{CH_4}$ from NASA. In the following (Section 3.1), we will present the various model sensitivity studies.

3.1 Sensitivity studies

Due to significant differences between the ~~EMEP~~ mOSaic scheme and the previous Wesely scheme with respect to implementation, it is not possible to fully disentangle and trace back every single difference in results to a respective change. Therefore, we conducted ~~in total nine sensitivity studies that mainly assess~~ one reference simulation denoted as *mOSaic* and in total seven sensitivity studies to probe the parameter space ~~of the stomatal conductance within the EMEP scheme~~for stomatal conductance (*mOSaic_offLight*, *mOSaic_offPhen*, and *mOSaic_SWVL1*), ozone surface resistance $R^{\mathrm{O_3}}$ (*mOSaic_ice*, *mOSaic_desert*, and *mOSaic_hough*), and emissions (*mOSaic_emis2014*). A reference simulation featuring the Oslo CTM3 Wesely scheme has been conducted and will be referred to as *Wesely_type*, indicating that other implementations of the original work by Wesely (1989) may exist in other models. All model experiments discussed in the following are summarized in Table 4. An *x* therein

Table 4. Summary of specifications of all simulations discussed in this section. For simplicity, only the tested parameters are listed. An x denotes that the model was run exactly in the configuration as has been described in Section 2.

...

† $R^{O_3}_{ice/snow} = 10000\,s\,m^{-1}$; * $R^{O_3}_{desert} = 800\,s\,m^{-1}$; * For adapted values see Supplement S.6

denotes that the model was run exactly in the configuration and with parameters as has been described in Section 2. For all model integrations, the meteorological reference year is 2005. This choice only affects the affects the direct comparison with data and multi-model studies that either perform analysis show results based on decadal averages or differing years. After finishing the work on the integration of the EMEP parameterization and initial testing, *EMEP_full* is the baseline simulation for the sensitivity studies, *EMEP_offLight* and *EMEP_offPhen*, because non-linearities in ozone formation and destruction make ozone concentrations sensitive to both, differences in local concentration of precursors and meteorological conditions (Jin et al., 2013).

First, we have a closer look at the influence of certain parameters on the stomatal conductance. As indicated by the names, these scenarios are extreme cases, *mOSaic_offLight* and *mOSaic_offPhen* are rather extreme scenarios completely switching off the sensitivity to light and phenology in Eq. (12) by setting f_{light} and f_{phen} to a fixed value of 1, respectively. During analysis of the results, we found, that the SMOKE-BEIS parameterization of the greening season did not extend to the boreal and subarctic regions. Especially in Europe, this basically results in a suppression of canopy resistance in northern Scandinavia. The following sensitivity study therefore comprises two different versions of pre-processed greening season (refer to Section 2.2 for details) : Mid and high latitudes in the northern hemisphere only (*EMEP_ppgs*) and for both, northern and southern hemisphere mid and high latitudes (*EMEP_ppgssh*). Building on the latterBecause of the underlying research project's focus on arctic and alpine ecosystems, where water might only be available from upper soil layers, an experiment was conducted using the uppermost soil water level (SWVL1) in the implementation of f_{SW}. After this, we want to confirm the importance of the $v^{O_3}_{ice/snow}$ update (Helmig et al., 2007) in the Subarctic and Arctics, within the framework of the Oslo CTM3 (choice of R^{O_3} for different land surface types. We conducted three experiments looking at a $R^{O_3}_{ice/snow}$ update (Helmig et al., 2007) (*mOSaic_ice*), observed $R^{O_3}_{desert}$ (Güsten et al., 1996) (*EMEP_ppgsshmOSaic_icedesert*). Accidentally, we have used , and an approximation of R^{O_3} originally used in *Wesely_type* (Wesely, 1989; Hough, 1991). Finally, we run a simulation with emissions for the year 2014 instead of 2005. Though, we take this as opportunity to assess the impact on ozone regarding differing emissions (*EMEP_ppgs_2005*). As mentioned previously, the simulations were initially conducted with the uppermost soil water level (SWVL1) in the implementation of f_{SW}. A final sensitivity study was conducted changing to soil water level at depths deeper than 1 m (*EMEP_SWVL4*). All simulations discussed in this section are summarized in Table 4. An x in the table denotes that the model was run exactly in the configuration as has been described in Section 22005 (*EMEP_emis2014*) to characterize the general influence of differing emissions on ozone.

In Fig. 4, we show the average relative difference between *EMEP_ppgsshmOSaic* and *Wesely_type* on global maps by means of surface ozone burden ozone burden in the lowermost model level, dry deposition velocity and total ozone dry de-

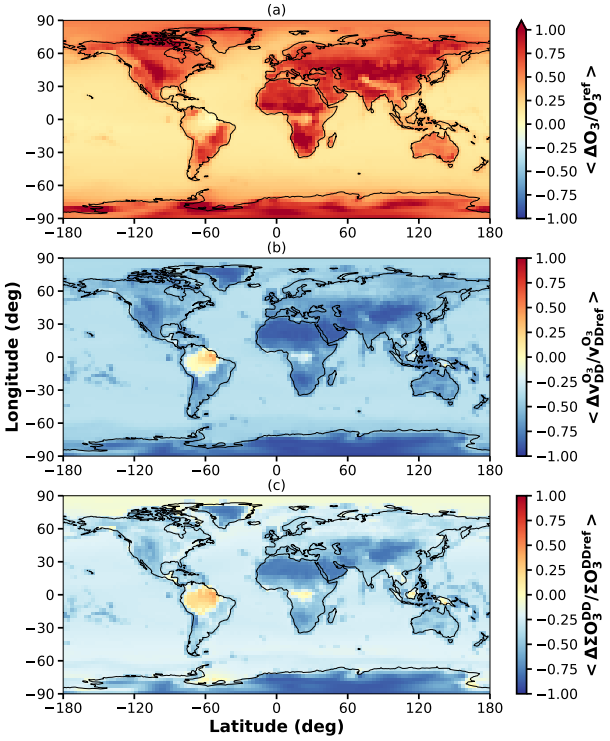

Figure 4. Relative difference between ~~the sensitivity simulation *EMEP_ppgsssh*~~ reference simulations *mOSaic* and the *Wesely_type* ~~in~~ with respect to (a) ~~total surface~~ average ozone burden in the lowermost model level; (b) average ozone dry deposition velocity; (c) total amount of ozone removed from the atmosphere by dry deposition.

position. ~~Surface ozone~~ The ozone burden increases globally except for some regions covered by tropical forest. Especially in desert regions in Africa, America, and Asia, ~~surface ozone increases by up to~~ ozone burden increases by more then 100 %. Consistently, dry deposition velocities decrease globally by the same order of magnitude in these regions, while they increase over tropical forest. With respect to total dry deposition, the picture is a bit less clear. We find a decrease of total dry deposition of ozone in desert regions and ocean covered areas and an increase in regions covered by tropical forest, while at mid and high latitudes in both hemispheres only small changes are visible. A possible explanation to this divergence especially in desert regions is the difference between the prescribed ~~dry deposition velocities~~ surface resistances R^{O_3} in the Wesely scheme in comparison to those used in ~~the EMEP scheme. We cover this in more detail in the following section~~*mOSaic*. We come back to this in the following sections.

3.2 Comparison with modeling results

In ~~our evaluation of results~~the evaluation of our model, we closely follow suggestions by Hardacre et al. (2015). For the purpose of comparison with the multi-model mean of the therein participating Task Force on Hemispheric Transport of Air Pollution (TF HTAP) models, we also have re-gridded our data to a horizontal resolution of $3° \times 3°$. In Section 3.2.1, we look at zonal distributions of ~~$[O_3](z_0)$~~$[O_3](p_0)$, $v_{DD}^{O_3}$, and $\sum O_3^{DD}$ for all our sensitivity simulations and study seasonal cycles of hemispheric ozone as well as for nine land surface types ~~which have been retrospectively separated~~ (Section 3.2.2). From this, we estimate the total annual ozone dry deposition onto ocean, ice, and land surfaces and compare also with results from Luhar et al. (2017).

~~As dry~~ Dry deposition velocities are ~~not directly available from the model output, monthly average~~ directly available only for the new model version. For *Wesely_type*, monthly averaged dry deposition velocities $v_{DD}^{O_3}$ ~~have been reconstructed~~ had to be retrospectively estimated from the ratio between the total ozone dry deposition ~~$\sum O_3^{DD}(z_0)$~~ $\sum O_3^{DD}(p_0)$ and monthly averaged ~~surface ozone amount $O_3(z_0)$~~ ozone amount in the lowermost model level $O_3(p_0)$

$$v_{DD}^{O_3} = \frac{\sum O_3^{DD}(z_0)}{O_3(z_0)} \frac{\sum O_3^{DD}(p_0)}{O_3(p_0)} \cdot c_{month}. \quad (29)$$

Herein, $c_{month} = \frac{\Delta h_{month}}{s_{month}}$, with the monthly average height of the lowermost model level in each gridbox Δh_{month} and the respective number of seconds in a month s_{month}. In case of *mOSaic*, resulting values for $v_{DD}^{O_3}$ from Eq. (29) are compatible with the values which are directly ailable from model output.

3.2.1 Zonal distribution

The annual zonal average with respect to surface ozone concentration (Fig. 5a) displays on average, in consistency with Fig. 4a, a global increase of surface ozone concentrations by ~~up to 10 ppb when applying the EMEP scheme compared to the Wesely scheme~~6 ppb comparing *mOSaic* to *Wesely_type*. This increase is largest in the zonal band $(25-50)°\mathrm{N}$ which contains the major deserts. In the deep tropics ($5°\mathrm{S}-5°\mathrm{N}$), the increase is smallest (~~$\Delta[O_3] \leq 5$ ppb~~$\mathcal{O}(5\,\mathrm{ppb})$). We find that the ~~EMEP~~ mOSaic scheme further intensifies the strong asymmetry between northern and southern hemisphere as a consequence of the distribution of the continental land masses and vegetation thereon. Among the sensitivity studies focusing on the stomatal conductance, there is only a low absolute variance. ~~Most remarkable, but expected due to the much smaller prescribed dry deposition velocity over ice and snow, *EMEP_ppgssh_ice* displays almost a doubling of surface ozone in the high Arctics compared to *Wesely_type* but affects ozone concentrations down to latitudes at about 50° in both hemispheres. Neglecting any dependence on solar radiation~~ Neglecting the dependence on light in the stomatal conductance formulation (~~*EMEP*~~*mOSaic_offLight*) – or in other words allowing photosynthesis 24/7 – ~~generally~~ decreases the ozone concentration by ~~about 2 ppb~~1 – 2 ppb in the tropics and NH mid latitudes, while choosing soil water at ~~deeper levels than the surface layer (~~shallower depths (~~*EMEP*~~*mOSaic_*~~*SWVL4*~~*SWVL1*) increases ~~$[O_3](z_0)$ slightly~~$[O_3]$ insignificantly. Rather surprisingly, switching off the phenology completely (~~*EMEP*~~*mOSaic_offPhen*) ~~, amounts~~ amounts on average only to small difference (~~at most 3.5 % increase in the deep tropics) . Switching from the SMOKE-BEIS parameterization to the pre-processed greening season (*EMEP_ppgs* compared to *EMEP_full*) , surface ozone increases on average~~ $\mathcal{O}(<1\,\mathrm{ppb})$). Most remarkable, but

expected due to the much smaller prescribed dry deposition velocity over ice and snow, *mOSaic_ice* displays a doubling of surface ozone in the high Arctics compared to *Wesely_type* ($\mathcal{O}(20\,\mathrm{ppb})$) but affects ozone concentrations down to latitudes at about 50° in both hemispheres. Reducing $R^{\mathrm{O_3}}_{\mathrm{desert}}$ by ~~6 % between (54 − 70) °N~~60 % (*mOSaic_desert*) a reduction in the order of 1 ppb is found mainly limited to the NH. The largest impact on ozone concentrations ($\mathcal{O}(2-5\,\mathrm{ppb})$) is found for the experiment *mOSaic_hough* which is closest to *Wesely_type*, since we used on average the same $R^{\mathrm{O_3}}$ (see Supplement S.6). The scenario of differing emissions (2005 in comparison to 2014 or more specifically ~~*EMEP_ppgs_2005*~~*mOSaic* compared to ~~*EMEP*~~*mOSaic_*~~*ppgs*~~*emis2014*), yields higher ozone concentrations in the northern hemisphere in 2005 in accordance to a reduction in sulfur and $\mathrm{NO_x}$ emissions in south east Asia in later years. An opposite tendency is seen for latitudes south of 30 °N, ~~probably owing to the industrial development of countries in these regions~~where an increase in ozone precursors is seen in CEDS.

The $v^{\mathrm{O_3}}_{\mathrm{DD}}$ are shown in Fig. 5b. The dry deposition velocities in the ~~EMEP scheme are on average 43 % lower than in~~ mOSaic scheme are well below the Wesely scheme and in remarkable agreement with the results shown by Hardacre et al. (2015). In the Arctics, except for ~~*EMEP_ppgssh*~~*mOSaic_ice*, all ~~realizations of the EMEP scheme are constantly~~ model experiments are slightly above the multi-model-mean. This indicates, that with respect to the other models, the ~~updated dry deposition velocity~~ Helmig et al. (2007) surface resistance above ice and snow should be considered as new standard for the Oslo CTM3. This may, however, lead to an overcompensation of the current arctic low-bias in surface ozone in the Oslo CTM3 and needs further evaluation. The dry deposition velocities are of course independent of the emission scenario, but display a strong ~~dependence~~ sensitivity on f_{light}~~and f_{phen}. The closer to 1 these factors are the higher the dry deposition velocities become (compare *EMEP_offLight*, *EMEP_offPhen*, and *EMEP_ppgssh*). That highlights the importance of a proper PAR from meteorological input in CTMs or radiative transfer in PAR in global climate models (GCMs) and a proper choice of phenology for canopy conductance computation. Albeit, the total numbers are smaller, the~~ , f_{phen}, and especially on the choice of $R^{\mathrm{O_3}}$. The shape of the normalized zonal average dry deposition velocities of the ~~EMEP scheme and the multi-model-mean are similar~~ mOSaic scheme are more similar to the multi-model-mean than to *Wesely_type* (Supplement S.7: Fig. S8). The biggest exceptions are the zonal bands $(50-70)\,^{\circ}\mathrm{S}$ ~~, which is~~ (almost entirely covered by ocean), $(12-30)\,^{\circ}\mathrm{S}$ ~~, which coincides~~ (coinciding with the location of Australia and its desert regions), as well as its counterpart in the northern hemisphere $(12-30)\,^{\circ}\mathrm{N}$. ~~However, it is not clear whether diverging dry deposition velocities over ocean or deserts have the larger impact.~~

The annual total ozone dry deposition is shown in Fig. 5c. In accordance to the previously described features, we observe a reduction of the global total ozone dry deposition in all sensitivity studies~~to almost~~ . In the most extreme case (NH subtropics and mid latitudes), the total ozone dry deposition drops to one-half of the amount given by *Wesely_type*. The occurrence of this reduction in the zonal bands, where the major deserts are located, points to a ~~change~~ substantial difference in $v^{\mathrm{O_3}}_{\mathrm{desert}}$. Consulting the parameter file used in the Wesely scheme, we indeed find $v^{\mathrm{O_3}}_{\mathrm{desert}} \equiv v^{\mathrm{O_3}}_{\mathrm{tundra}} = 0.26\,\mathrm{cm\,s^{-1}}$ (Hough, 1991), while in the ~~EMEP~~ mOSaic scheme $v^{\mathrm{O_3}}_{\mathrm{desert}} = 0.05\,\mathrm{cm\,s^{-1}}$ and $v^{\mathrm{O_3}}_{\mathrm{tundra}} = 0.24\,\mathrm{cm\,s^{-1}}$, respectively. Similarly, dry deposition velocities over ice and snow and ocean have been even higher in the Wesely scheme ($v^{\mathrm{O_3}}_{\mathrm{ice/snow}} \equiv v^{\mathrm{O_3}}_{\mathrm{water}} = 0.07\,\mathrm{cm\,s^{-1}}$) than in the original ~~EMEP scheme ($v^{\mathrm{O_3}}_{\mathrm{ice/snow}} \equiv v^{\mathrm{O_3}}_{\mathrm{water}} = 0.05\,\mathrm{cm\,s^{-1}}$)~~parameter set ($v^{\mathrm{O_3}}_{\mathrm{ice/snow}} \equiv v^{\mathrm{O_3}}_{\mathrm{water}} = 0.05\,\mathrm{cm\,s^{-1}}$, Simpson et al., 2012). These differences in ~~baseline dry deposition velocities~~ surface resistances over huge parts of the unvegetated surface of the

Earth ~~amount to~~ accounts for most of the ~~quantitative~~ qualitative difference between the Wesely and the ~~EMEP scheme~~mOSaic scheme, but does not explain the quantitative difference (compare *mOSaic_hough*). We further elaborate on this in the following ~~section~~ (Section 3.2.2).

There seems to be a discrepancy between the Oslo CTM3 response and the multi-model-mean, since the Wesely scheme is similar to the multi-model-mean with respect to total annual ozone dry deposition, while the ~~reconstructed~~ $v_{\mathrm{DD}}^{\mathrm{O_3}}$ of the ~~EMEP~~ mOSaic scheme match better. This could be a sign of differences in photo-chemistry and transport (e.g. convective, advective, STE) between the Oslo CTM3 and the average TF HTAP model, but without comparing to the actual ~~$[\mathrm{O_3}(z_0)]$~~ $[\mathrm{O_3}]$ of the TF HTAP models that participated in the model intercomparison, we cannot elaborate on this any further. This may also hint to issues in the Oslo CTM3 photo-chemistry, which may have a too high ozone production, or the actual removal of ozone from the atmosphere, which might have been adjusted to the less physical dry deposition velocities in the past, but this is subject to further investigations.

In Appendix Fig. A1a, the average zonal ozone dry deposition is shown separated by month. Where available, we have added the multi-model-mean given by Hardacre et al. (2015) as reference. ~~There~~ As for the global annual comparisons above, the mOSaic scheme matches the multi-model-mean values remarkably well with respect to dry deposition velocities, while it strongly underestimates the total dry deposition. Qualitatively, there are two major phases apparent: NH and SH greening season. Spring and summer in the NH is reflected in a pronounced peak of $v_{\mathrm{DD}}^{\mathrm{O_3}}$ in the northern mid latitudes, while it is absent in winter (SH summer). Spring and summer in the SH are marked by a southward shift of the tropical peak dry deposition velocity and a slight increase of $v_{\mathrm{DD}}^{\mathrm{O_3}}$ in the region $(20-40)\,^{\circ}\mathrm{S}$. In the Wesely scheme, NH mid latitude peak velocities appear in June compared to July in the ~~EMEP~~ mOSaic scheme, indicating that the seasonal cycles differ. The corresponding total monthly ozone dry deposition is shown in Appendix Fig. A1b. In general, the seasonal patterns are quite similar in the Wesely scheme and the ~~EMEP~~ mOSaic scheme, displaying a strong symmetry around $10\,^{\circ}\mathrm{N}$ in January/February and November/December, respectively. What differs most is the molding and intensity of the NH peak dry deposition. Both schemes reach the maximum in June/July but the peak is much more differentiated in March already in the Wesely scheme. Similarly, the SH tropical peak dry deposition is reached in August/September but sustained longer, into October, in the Wesely scheme. Since we have not conducted any simulation with a meteorological year other than 2005, we cannot elaborate on whether this is a special feature of our chosen year or not. ~~In comparison, the available 2 months of the multi-model-mean display a somewhat different pattern. Especially the NH/SH asymmetry is much more pronounced in February, than it is the EMEP scheme.~~

3.2.2 Average seasonal cycles

To further disentangle the contributions of different regions to the global ozone budget, we will ~~briefly~~ look at different projections of seasonal cycles.

In Fig. 6, the total annual ozone dry deposition separated into mid and high latitudes in the northern hemisphere ($30\,^{\circ}-90\,^{\circ}\mathrm{N}$), the tropics and subtropics ($30\,^{\circ}\mathrm{S}-30\,^{\circ}\mathrm{N}$), and the mid and high latitudes in the southern hemisphere ($30\,^{\circ}-90\,^{\circ}\mathrm{S}$) is shown. We have added the multi-model-mean by Hardacre et al. (2015) as reference. While the total ozone dry deposition

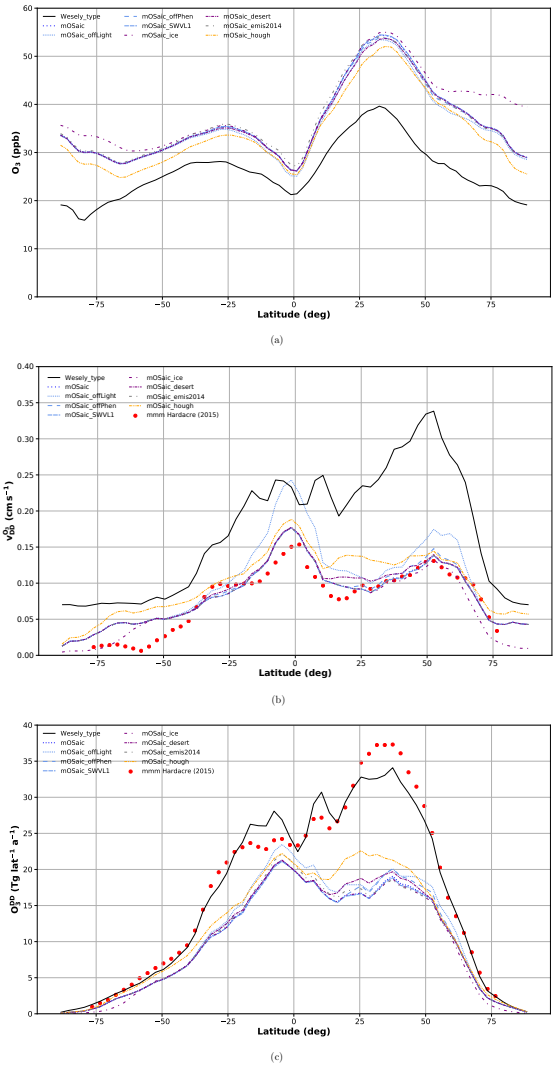

Figure 5. Comparison of the manifold of Oslo CTM3 integrations with respect to (a) ~~Surface ozone~~ Ozone concentrations in the lowermost model level, (b) Annual average ozone dry deposition velocity, (c) Total annual ozone dry deposition. The different colors indicate sets of simulation with similar baselines. The multi-model mean from the evaluation of TF HTAP models by Hardacre et al. (2015) is shown as a reference (where available).

of *Wesely_type* agrees well with the multi-model-mean in any zonal band, the mOSaic scheme displays a much smaller total ozone dry deposition. This deviation appears to be almost the same for each zonal band ($6-7\%$).

As expected, the NH mid and high latitudes display a strongly pronounced seasonal cycle, while it is less pronounced in the tropics (due to the lack of seasons) and in the SH (due to the small percentage of vegetated surface). The highest ozone dry deposition is found in the tropics and amounts on average to the peak level of dry deposition in the NH for the

multi-model-mean (Hardacre et al., 2015) and ~~EMEP~~ mOSaic scheme. In the Wesely scheme, the average tropical ozone dry deposition diverges by ~~about~~ 5 Tg in comparison to its corresponding NH maximum. ~~The~~ Compared to the multi-model-mean, the seasonal cycle in the ~~EMEP scheme~~ Oslo CTM3 NH appears to be shifted towards later in the year~~in the NH~~. The seasonal cycle in the tropics and subtropics ~~is not changing, but the~~ only differs by magnitude otherwise the shapes are identical for both the mOSaic scheme, the Wesely scheme, and the multi-model-mean. The total amount of dry deposition of ozone ~~is very sensitive to differing realizations of the EMEP scheme, with~~ differs strongly between the different model experiments, with ~~*EMEP*~~*mOSaic*_~~*offLight*~~*SWVL1* and ~~*EMEP_ppgs*~~*mOSaic*_~~*2005hough*~~ displaying the ~~highest and the lowest~~ lowest and highest amount, respectively. This indicates that surface ozone is much more sensitive to the choice of parameters ($\mathcal{O}(5\,\mathrm{ppb})$ for *mOSaic_hough* in the tropics~~may be very sensitive to changes in emissions of ozone precursors and changes in long-wave radiative transfer (e.g., due changes in cloud cover or aerosol~~) than to slight changes in precursor emissions ($\mathcal{O}(1\,\mathrm{ppb})$ for *mOSaic_emis2014* in the tropics).

As suggested by Hardacre et al. (2015), we ~~retrospectively separate~~ also look at ozone dry deposition velocities with respect to surface types separately. Since dry deposition velocities are not directly available for *Wesely_type*, we use Eq. (29) to estimate these. Based on a CLM 2 average dynamic land surface map, we ~~generated~~ generate masks for 9 different surface types (Fig. B1a~~and used~~) and use these to select gridboxes with a high percentage of these surface types, ranging from a meager 70 % for cropland in the NH mid latitudes to 100 % regarding desert, ocean, snow and ice, and tropical forest. Thus, it ~~was~~ is not possible to exclusively select gridboxes with 100 % cover for each surface type. Since we have not performed a full unfolding on the data, the results should be treated with slight caution (e.g. over cropland). In case of the mOSaic scheme, we have pre-selected the dry deposition velocities in accordance to the land surface type.

In Fig. 7, the seasonal cycles of dry deposition velocities are shown for the nine surface categories. The patterns and absolute numbers differ substantially between the Wesely scheme and the ~~EMEP~~ mOSaic scheme and the multi-model-mean. The divergence of the average dry deposition velocities between ~~the Wesely scheme and the EMEP scheme~~ *Wesely_type* and *mOSaic* in desert regions ($\Delta\overline{v}^{\mathrm{O_3}}_{\mathrm{desert}} = 0.18\,\mathrm{cm\,s^{-1}}$ $\Delta\overline{v}^{\mathrm{O_3}}_{\mathrm{desert}} = 0.20\,\mathrm{cm\,s^{-1}}$) as well as grassland ($\Delta\overline{v}^{\mathrm{O_3}}_{\mathrm{grassland}} = 0.54\,\mathrm{cm\,s^{-1}}$ $\Delta\overline{v}^{\mathrm{O_3}}_{\mathrm{grassland}} = 0.65\,\mathrm{cm\,s^{-1}}$) is quite remarkable~~as well as the difference of both~~ . The difference of *mOSaic* and *Wesely_type* to the multi-model-mean in tropical forest regions (~~$\Delta\overline{v}^{\mathrm{O_3}}_{\text{tropical forest}} = 0.49\,\mathrm{cm\,s^{-1}}$~~). ~~In contrast to the Wesely scheme and the EMEP scheme, the~~ is $\Delta_{\text{mOSaic}}\overline{v}^{\mathrm{O_3}}_{\text{tropical forest}} = 0.61\,\mathrm{cm\,s^{-1}}$ and $\Delta_{\text{Wesely\_type}}\overline{v}^{\mathrm{O_3}}_{\text{tropical forest}} = 0.49\,\mathrm{cm\,s^{-1}}$, respectively. The multi-model-mean ~~indicates~~ displays a rather pronounced seasonal cycle in desert regions ($0.10\,\mathrm{cm\,s^{-1}} \leq v^{\mathrm{O_3}}_{\mathrm{desert}} \leq 0.15\,\mathrm{cm\,s^{-1}}$)~~. The estimated~~ , which cannot be reproduced with the mOSaic scheme. The dry deposition velocities over desert regions are consistent with the ~~previously mentioned baseline values of ozone dry deposition~~average values from the prescribed ozone surface resistances, which means that in the ~~EMEP~~ mOSaic scheme they are ~~about~~ 1 order of magnitude lower than in the Wesely scheme. In the mOSaic scheme, dry deposition to deserts is dominated by contribution from R_b. From a limited number of ozone flux measurements in the Sahara desert, Güsten et al. (1996) deduced $v^{\mathrm{O_3}}_{\text{desert, day}} = 0.1\,\mathrm{cm\,s^{-1}}$, $v^{\mathrm{O_3}}_{\text{desert, night}} = 0.04\,\mathrm{cm\,s^{-1}}$, and $\overline{v}^{\mathrm{O_3}}_{\mathrm{desert}} = 0.065\,\mathrm{cm\,s^{-1}}$. This implies, that ozone dry deposition over desert regions is highly overestimated in the Wesely scheme as well as in TF HTAP models, while it may be underestimated in the ~~EMEP~~ mOSaic scheme. Similarly, the dry deposition velocities over water differ. From measurements during ship-campaigns a mean value of $\overline{v}^{\mathrm{O_3}}_{\mathrm{water}} = 0.019\,\mathrm{cm\,s^{-1}}$ over the ocean

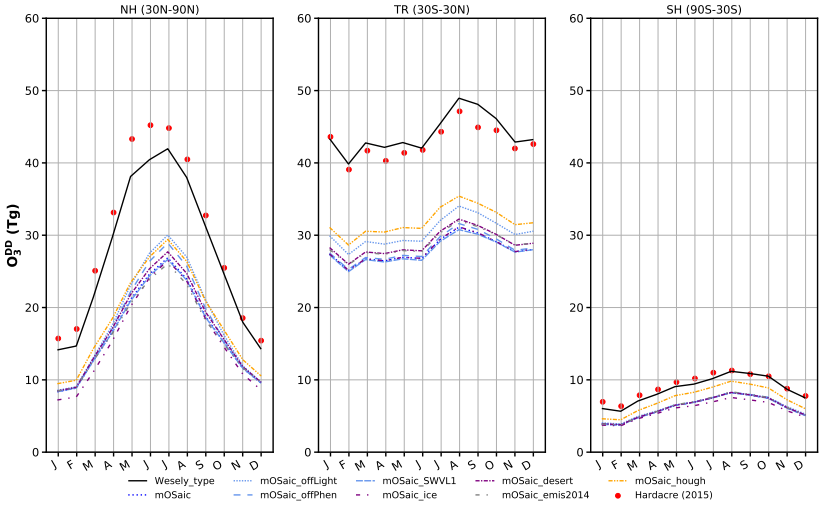

Figure 6. Seasonal cycle of total annual amount of ozone removed from the atmosphere through dry deposition separated into northern hemisphere (NH), tropics (TR), and southern hemisphere (SH). The multi-model mean from the evaluation of HTAP models by Hardacre et al. (2015) is shown as a reference.

has been deduced (Helmig et al., 2012). In a model study of different mechanisms of dry deposition to ocean waters by means of prescribed $\overline{v}^{O_3}_{water}$ and one- and two-layer gas exchange modeling, Luhar et al. (2017) found $\overline{v}^{O_3}_{water}$ ranging between $0.018\,cm\,s^{-1}$ (two-layer scheme) and $0.039\,cm\,s^{-1}$ (prescribed). With $\overline{v}^{O_3}_{water} = (0.046 \pm 0.002)\,cm\,s^{-1}$, the ~~EMEP~~ mOSaic scheme (Section 2.1.2) yields probably a too strong dry deposition to ocean~~which~~ , but is in line with the multi-model-mean. This implies that ozone concentrations might even become larger and dry deposition even lower in the model if a ~~two-layer scheme~~ more advanced dry deposition scheme to the ocean would be implemented. With respect to vegetation, we might be able to improve the model performance further by allowing more PFTs and phenologies, especially in regions covered by tropical ~~or coniferous forest (Anav et al., 2017)~~ forest (Anav et al., 2017) or in boreal regions.

Finally, we take a look at the different global as well as hemispheric dry deposition sinks for ozone (Table 5). Despite its vastness, the ocean amounts only to ~~about 23 %~~ 35 % of the global ozone sink due to dry deposition in the Oslo CTM3 with operative ~~EMEP scheme , while~~ mOSaic scheme (*mOSaic*), while permanently ice and snow ~~account for far less than 1 %~~covered regions account for 1.2 %. The remainder is deposited to ~~various other~~ land surfaces of which deserts might be the most neglected in process-modeling. The total annual dry deposition in the ~~EMEP scheme is about~~ mOSaic scheme is one-third below the multi-model-mean result by Hardacre et al. (2015). But also the results of ~~Luhar et al. (2017)~~ Luhar et al. (2017, 2018) yield a $(19 - 27)\,\%$ lower ozone dry deposition than the models participating in the model intercomparison, with deposition to ocean ranging between $(12 - 21)\,\%$ of the total annual ozone dry deposition. In particular, Luhar et al. (2018) found that current model estimates of ozone dry deposition to the ocean may be three times too high compared to their analysis. This implies that the ozone dry deposition to the ocean the Oslo CTM3 is too high as well.

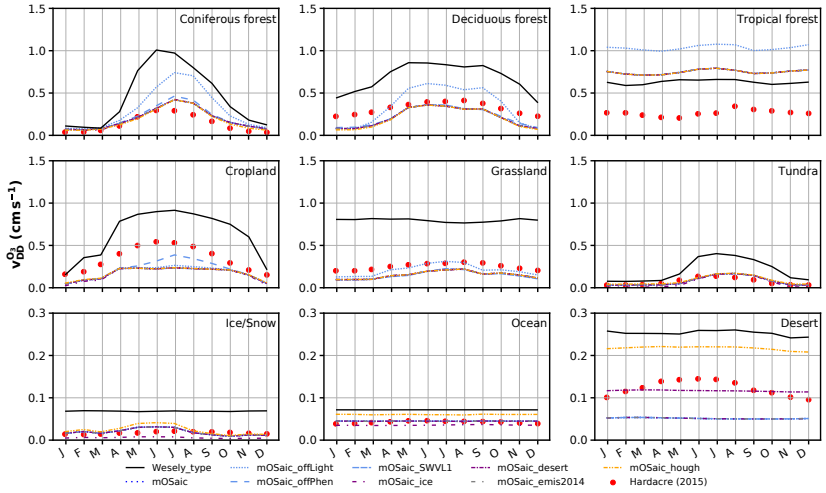

Figure 7. Average seasonal cycles of ozone dry deposition velocities separated by land use type. Results from (Hardacre et al., 2015) are shown as a reference. We refrain from showing the full extent of *EMEP_offLight* here, since it is an extreme scenario and has been discussed already.

Table 5. Total ozone dry deposition for the respective ~~year~~ model experiment in Tg a^{-1} ~~separated into~~ . The global ozone dry deposition has been weighted by ocean, ice and, land ~~contributions~~fraction in each gridbox, respectively. *Ice* herein refers to regions at high latitudes that are permanently covered by ice and snow.

Experiment	Ocean			Ice			Land		
	NH	SH	Global	NH	SH	Global	NH	SH	
	(Tg a^{-1})			(Tg a^{-1})			(Tg a^{-1})		
Wesely_type	~~88.7~~ 160.5	~~110.3~~ 147.7	~~199.0~~ 308.2	~~0.7~~ 7.0	~~5.0~~ 6.4	~~5.7~~ 13.4	~~346.1~~ 417.3	~~153.5~~ 190.8	
~~EMEP_full~~ mOSaic	~~67.1~~ 108.1	~~84.7~~ 105.3	~~151.8~~ 213.4	~~0.6~~ 4.3	~~4.4~~ 3.1	~~5.0~~ 7.4	~~236.0~~ 236.2	~~112.3~~ 130.3	
~~EMEP~~mOSaic_offLight	~~66.6~~ 110.5	~~84.1~~ 106.3	~~150.7~~ 216.8	~~0.6~~ 4.3	~~4.4~~ 3.0	~~5.0~~ 7.4	~~267.8~~ 263.1	~~129.8~~ 145.3	
~~EMEP~~mOSaic_offPhen	~~67.1~~ 108.3	~~84.6~~ 105.3	~~151.7~~ 213.6	~~0.6~~ 4.3	~~4.4~~ 3.1	~~5.0~~ 7.4	~~239.9~~ 246.9	~~116.0~~ 132.2	
~~EMEP_SWVL4~~ mOSaic_SWVL1	~~68.1~~ 108.1	~~86.1~~ 105.2	~~154.2~~ 213.3	~~0.6~~ 4.3	~~4.5~~ 3.1	~~5.1~~ 7.4	~~241.8~~ 234.6	~~115.0~~ 128.8	
~~EMEP_ppgs~~ mOSaic_ice	~~67.1~~ 105.6	~~84.6~~ 103.0	~~151.7~~ 208.6	~~0.6~~ 2.6	~~4.4~~ 1.0	~~5.0~~ 3.6	~~238.7~~ 232.7	~~112.6~~ 130.2	
~~EMEP_ppgssh~~ mOSaic_desert	~~67.0~~ 109.1	~~84.5~~ 105.5	~~151.6~~ 214.6	~~0.6~~ 4.3	~~4.4~~ 3.1	~~5.0~~ 7.4	~~243.9~~ 250.4	~~119.4~~ 132.6	
~~EMEP_ppgssh_ice~~ mOSaic_emis2014	~~66.5~~ 108.9	~~84.8~~ 107.0	~~151.3~~ 215.9	~~0.2~~ 4.3	~~1.3~~ 3.1	~~1.4~~ 7.3	~~240.3~~ 238.3	~~120.4~~ 133.8	
~~EMEP_ppgs_2005~~ mOSaic_hough	~~66.8~~ 133.3	~~83.5~~ 131.1	~~150.4~~ 264.4	~~0.6~~ 4.9	~~4.4~~ 3.6	~~5.0~~ 8.4	~~237.8~~ 265.8	~~110.0~~ 132.0	

†: Relative change of global annual total in comparison to *mOSaic*.

Table 6 displays the average tropospheric ozone burden for all model experiments. Consistently with the previous findings, the mOSaic scheme increases the tropospheric ozone burden by 35 Tg. From various satellite ozone retrieval products, Gaudel et al. (2018, T

deduce a lower limit estimate for global tropospheric ozone burden for the years 2010 – 2014 of 333 – 345 Tg, but remark that this amount underestimates the actual tropospheric ozone burden, since it is only based on daytime retrievals. Nevertheless, the results of *mOSaic* lie 17 % above that estimate and also well above the typical modeling range of 302 – 378 Tg (Young et al., 2013). Despite the strong positive bias in ozone concentrations and accordingly low-bias in total dry deposition, the difference between *mOSaic* and *mOSaic_emis2014* (6 Tg), lies well within the range given by satellites for the years 2005 and 2014 (Gaudel et al., 2018, Fig. 26). This indicates that the Oslo CTM3 responses well to given changes in global emissions.

Table 6. Annual mean tropospheric ozone burden for all experiments and 1σ standard deviation.

Experiment	Trop. O_3 (Tg)		
Wesely_type	364	±	23
mOSaic	399	±	31
mOSaic_offLight	395	±	30
mOSaic_offPhen	398	±	31
mOSaic_SWVL1	399	±	31
mOSaic_ice	401	±	31
mOSaic_desert	398	±	31
mOSaic_emis2014	405	±	32
mOSaic_hough	393	±	30

3.3 Comparison with ~~observations~~MACC-reanalysis

In this section, we conclude the comparison of our results with respect to global ozone by looking at ECWMF's MACC-reanalysis (MACC-II Consortium, 2011, data obtained from ECWMF's data center). In Fig. 8, we compare *mOSaic* ozone concentrations in the lowermost model level with surface concentrations deduced from the MACC-reanalysis for the year 2005. The MACC-reanalysis displays low ozone concentrations above all land masses except for the Greenland ice sheet. The lowest values are found in the deep tropics (e.g. northern South America and central Africa), while the highest values occur within (25 – 60) °N over the oceans. These low values over the oceans are relatively well reproduced by *mOSaic* (±20 %). Over, e.g., South America, central and southern Africa, the Arabian peninsula, and the north-western Indian subcontinent, the ozone concentrations are elevated by up to 200 %. While on global average much more concise with the MACC-reanalysis, *Wesely_type* displays a similar tendency with respect to elevated ozone over continents. Enhanced ozone compared to MACC-reanalysis is found in the deep tropics and the north-western Indian subcontinent (Supplement S.8) which coincides with regions of high intensity in incoming UV radiation. This may indicated an imbalance in the photo-chemical production and loss of O_3 in the Oslo CTM3.

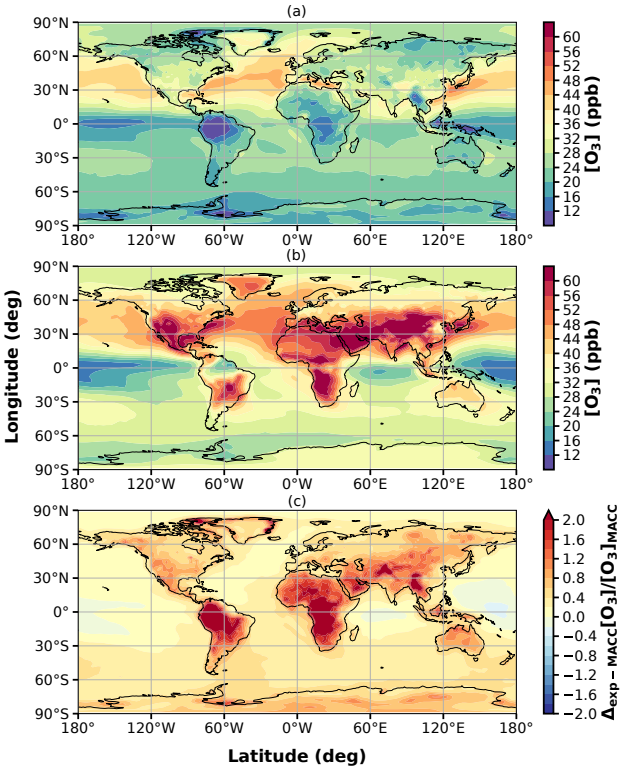

Figure 8. Mean ozone concentrations for the year 2005. (a) MACC-reanalysis (surface); (b) Oslo CTM3 *mOSaic* (lowermost model level); (c) Relative difference.

3.4 Comparison with ground-based observations

In this section, we compare our model results to observations at a selected number of sites which provide ozone flux measurements. For all comparisons, we use the original resolution of the Oslo CTM3 ($2.25° \times 2.25°$) instead of the re-gridded resolution ($3° \times 3°$).

In Fig. 9a, seasonal cycles of average ozone dry deposition fluxes for ~~six~~ the six selected observation sites are shown. We have computed a model average for all sensitivity studies at the closest grid point and show the $1\,\sigma$ ~~error~~ uncertainty band. The shaded area around the multi-model-mean indicates the broad range of model results but is not an actual ~~error~~ uncertainty band since such is not given in Hardacre et al. (2015). At ~~about~~ 4 of 6 sites, the ~~EMEP~~ mOSaic scheme performs better than the Wesely scheme and ~~better than or the same as~~ similar to or better than the multi-model-mean. We use a χ^2-test

$$\chi^2 = \sum_{i=1}^{12} \frac{\left(\overline{\mathrm{O}}^{\mathrm{sim}}_{3\mathrm{DD},\,i} - \overline{\mathrm{O}}^{\mathrm{obs}}_{3\mathrm{DD},\,i}\right)^2}{\sigma_i^2}, \tag{30}$$

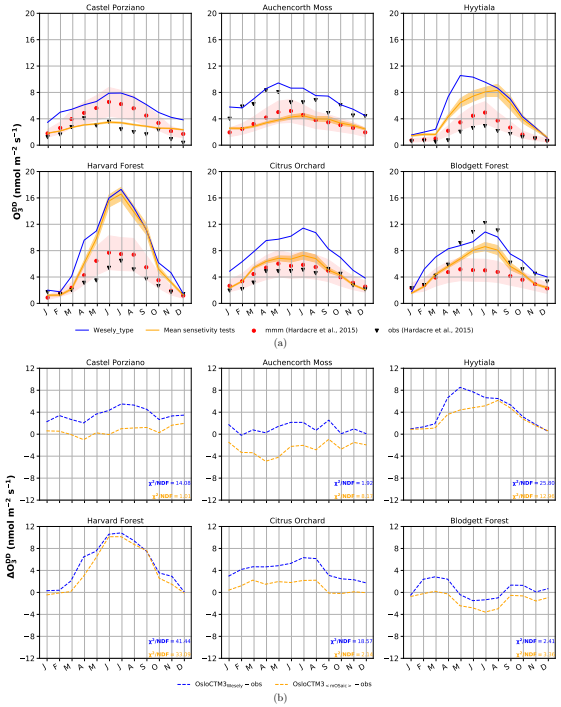

Figure 9. Ozone dry deposition fluxes at different observation sites. (a) Comparison between Wesely scheme and average result from all sensitivity studies with observational averages taken from Hardacre et al. (2015). The model uncertainty of the Oslo CTM3 is given as 1σ error band. The shaded area around the multi-model-mean indicates the broad range of different model results but is not an actual error band. (b) Model divergence from observation and χ^2-test results.

with an estimated standard deviation of observation $\sigma_i = 1\,\mathrm{mmol\,m^{-2}\,s^{-1}}$ and divide it by the number of degrees of freedom (NDF) to assess this subjective analysis in a more objective way. The closer to 1 this test scores, the better does the simulation represent the observation. A score between 0 and 1 indicates that the estimated σ is too small. The results of the χ^2-test are shown together with the divergences in Fig. 9b. The χ^2-test reveals also that in 4 of 6 cases the ~~EMEP~~ mOSaic scheme improves the performance of the Oslo CTM3 with respect to observed ozone dry deposition fluxes, although a satisfying result is only achieved for two sites (Castel Porziano, Blodgett Forest). With only one full year of simulation, the model uncertainty regarding the seasonal cycle at observational sites cannot be properly quantified. Furthermore, the observational averages comprise at most 9 years worth of data. Statistically, these data may still be subject to interannual variability. Among other aspects, the horizontal as well as vertical resolution play an important role in the model performance. Although, we do not explicitly assess the impacts of differing resolutions in our model, we can assume that both high and low biases exist due to dilution of sources and sinks in coarse resolution models (Schaap et al., 2015). Good matches between observation and model are only to be expected if the station's location is representative for an area similar to the respective model gridbox and not substantially affected by differences in modeled and actual topography (e.g., major wind directions).

4 Summary and conclusions

We have presented an update of the dry deposition scheme in the Oslo CTM3 from purely prescribed dry deposition velocities (Wesely, 1989; Hough, 1991) to a more process-oriented parameterization taking the state of the atmosphere and vegetation into account~~(Simpson et al., 2012). In our implementation based on Simpson et al. (2012), we follow a classical, resistance analogous approach in computing~~. Based on the description of dry deposition in Simpson et al. (2003, 2012), we have implemented a moasic approach to compute contributions to dry deposition ~~. The~~ by individual sub-grid land surface types. Aerodynamic, quasi-laminar~~resistance in the dry deposition scheme is capable of adjusting to surface wind stress but falls back to its prescribed limits in most of the tested cases. The surface resistance computation is~~, and surface resistance (latter divided into stomatal and non-stomatal ~~resistance. The stomatal resistance is sensitive to parameters associated with the vegetation such as photosynthetic active radiation, water vapor pressure deficit, soil water content, and plant phenology, while the non-stomatal resistance is affected by the existence or absence of vegetation~~contributions) are calculated for each land surface category separately. Based on these, a land fraction-weighted mean is deduced. In addition, the various dry deposition velocities are now directly available from model output for diagnostics and further studies.

The new dry deposition scheme named *mOSaic* improves the modeled dry deposition velocities which are now compatible with observation and model studies (e.g., Hardacre et al., 2015; Luhar et al., 2018). Dry deposition velocities are reduced by $6-60\,\%$. At the same time, the annual amount of ozone dry deposition decreases by ~~up to~~ more than $100\,\%$ ~~changing from the old dry deposition scheme to the new one~~over all major desert areas and increases over tropical forest. Compared to results from a multi-model evaluation (Hardacre et al., 2015), the total annual ozone dry deposition in the Oslo CTM3 is ~~about $33\,\%$~~ $(38^{+\frac{1}{10}})\,\%$ below average. However, there seems to be a tendency that newer TF HTAP models show a lower total annual dry deposition of ozone than older models, indicating that newer developments lead to decreasing ozone dry deposition and increasing tropospheric ozone burden ~~(e.g., Luhar et al., 2017; Hu et al., 2017)~~(e.g., Luhar et al., 2017, 2018; Hu et al., 2017).

We found the response of the Oslo CTM3 to the changes in dry deposition velocities from the old and the ~~new dry deposition~~ mOSaic scheme to be consistent. A decrease in $v_{\mathrm{DD}}^{\mathrm{O_3}}$ leads to a decrease in total ozone dry deposition and an increase in ~~surface ozone concentration $[\mathrm{O_3}(z_0)]$~~ozone concentration $[\mathrm{O_3}]$. As the new scheme is quantitatively more similar to the multi-model-mean (Hardacre et al., 2015) with respect to dry deposition velocities, while the old scheme agrees better in terms of total dry deposition, there is an apparent discrepancy~~when comparing with the multi-model-mean. Without knowing $[\mathrm{O_3}(z_0)]$ of the TF HTAP models, this cannot be~~. By means of tropospheric ozone burden (Gaudel et al., 2018) and surface ozone concentrations deduced from the MACC-reanalysis (MACC-II Consortium, 2011), the Oslo CTM3 with operational mOSaic scheme shows a pronounced high-bias of tropospheric ozone. While the average bias is small or even reversed when using the old scheme, both display elevated ozone in comparison with the MACC-reanalysis in continental regions with high average incoming UV radiation (e.g., northern South America, central and southern Africa, the Himalayas). The reason behind this bias has not yet been resolved and may hint to, e.g., ~~differences~~ issues in photo-chemistry ~~, stratosphere-troposphere-exchange as well as to differences in aerosol loadings among many other aspects~~([OH] related ozone production and loss) or previously introduced optimization of ozone removal with respect to the old, less physical dry deposition velocities.

Most of the ~~decrease~~ qualitative change in ozone dry deposition in the Oslo CTM3 ($-2-12\,\%$) can be attributed to changes in dry deposition ~~velocities~~ over the ocean and deserts. This is mainly due to updates of the respective~~prescribed dry deposition velocities~~ $v_{\mathrm{DD}}^{\mathrm{O_3}}$, prescribed ozone surface resistances $R^{\mathrm{O_3}}$. In case of desert and grasslands the difference between the old and new prescribed value is ~~at~~ in the order of 1 magnitude. Over the ocean, the absolute change in dry deposition is small, but it is accumulated over a large area which is especially amplified in the southern hemisphere. Small adjustments to the lower limits in our quasi-laminar layer resistance formulation may help improve the Oslo CTM3 performance in this regard. With respect to available measurements of dry deposition velocities of ozone over desert (Güsten et al., 1996) and ocean (Helmig et al., 2012), the new Oslo CTM3 dry deposition scheme slightly underestimates ozone dry deposition velocities over the former and overestimate them over the latter. Regarding the vastness of the ocean and the ongoing desertification, it may be worthwhile to ~~study dry deposition in these regimes at a~~ revise the dry deposition scheme for these regimes and add more process-oriented ~~level~~formulations, e.g., 2-layer gas exchange with ocean waters ~~(Luhar et al., 2017)~~(Luhar et al., 2017, 2018), wave braking and spray (Pozzer et al., 2006).

Although dry deposition to ice and snow amounts to ~~less than~~ only $1\,\%$ of the total global annual ozone dry deposition in *mOSaic*, a decrease in prescribed dry deposition velocity in accordance to combined measurements and model studies (Helmig et al., 2007) causes almost a doubling in the surface ozone concentrations in the high Arctics and affects surface ozone concentrations down to latitudes at ~~about~~ $50\,^\circ$ in both hemispheres. ~~By comparing~~ Comparing with results from the multi-model evaluation (Hardacre et al., 2015), we conclude that it is important to use this updated ozone dry deposition velocity to counter an Arctic surface ozone low-bias in ~~the model~~models, however, this ~~could lead~~ currently leads to an overcompensation (high-bias) in the Oslo CTM3.

We have studied the parameter space of the stomatal conductance parameterization and found that total surface ozone in the tropics and the northern hemisphere is most sensitive to changes ~~in ozone uptake by plants. The difference between our~~ therein. In the most extreme test ~~cases amounts to $15\,\%$ with respect to total surface ozone~~case, the increase in global total dry deposition amounts to $7.3\,\%$, while the more realistic test ~~case~~ cases, e.g. using differing years of emission ~~amounts to about $5\,\%$~~amount to changes in the order of $\pm 2\,\%$. This may indicate that future changes in vegetation cover and solar radiation at the surface due to changes in stratospheric ozone, cloud cover, or aerosols could also strongly influence the surface ozone burden in the tropics. Total column ozone in the tropics is predicted to decrease due to changes in the atmospheric circulation (e.g., WMO - Global Ozone Research and Monitoring Project, 2014), while tropospheric and surface ozone increase. The combined effects of increasing emissions of ozone precursors and an increase in UV due to thinning of stratospheric ozone might permit more UV light at ground and thus increase the ozone production.

~~In the northern hemisphere mid and high latitudes ($50\,^\circ - 75\,^\circ$N), total surface ozone increases by about $7.7\,\%$ if the beginning and end of the vegetation period is estimated based on a $5\,^\circ$C-days criteria instead of prescribed. This is very important for any study focusing on ozone in the boreal and subarctic regions.~~

An important factor in the global ozone budget are emissions of precursor substances. We cover this by using the same meteorology with different years of CEDS emissions. We chose the years 2005 and 2014 for our comparison. Ozone precursor emissions in 2014 are slightly lower in the NH while enhanced in the tropics and the SH. In 2014, surface ozone burden is

higher in the southern hemisphere and in the tropics (~~$\sim 5\,\%$~~$5\,\%$) compared to 2005, while it is lower in the northern hemisphere (~~$\sim 2\,\%$~~). ~~This is most likely reflecting the ongoing industrialization process of countries in the southern hemisphere and the commitment and implementation of air quality regulations of industrialized nations in the northern hemisphere.~~ $2\,\%$).

We also evaluated the model with respect to observed dry deposition ~~velocities~~ fluxes at six sites in the northern hemisphere and found that the ~~updated dry deposition~~ mOSaic scheme performs better than the old one, but is not able to reproduce the measurements at most sites quantitatively. This may be due to several reasons. The model resolution in both horizontal ($2.25^\circ \times 2.25^\circ$) and vertical (L60, $P_{\mathrm{max}} = 0.02\,\mathrm{hPa}$) does not capture all details in transport, thus affecting the distribution and transport (e.g., long-range, convection, and stratosphere–troposphere exchange) of ozone and its precursors. Depending on the location of the observation site and its respective representativeness for a larger area, ozone dry deposition and ozone concentrations are expected to be over- or underestimated in the model. Because of non-linearities in ozone formation and destruction, ozone concentrations are sensitive to both, differences in local concentration of precursors and meteorological conditions (Jin et al., 2013). In addition, a comparison of very few years of measurement to only one specific year of simulation may reflect the year to year variability more than the actual model performance.

Future work on the Oslo CTM3 should ~~include a direct output of dry deposition velocities for diagnostic purposes. The~~ resolve the ozone high-bias which may involve revising the photolysis- and chemical reaction computation as well as reaction rates. For a better modeling of ozone abundances, ocean emissions of very short-lived ozone depleting substances (VSLS) (Warwick et al., 2006; Ziska et al., 2013) which affect the stratospheric ozone (Hossaini et al., 2016; Falk et al., 2017) and a scheme covering arctic spring-time ozone depletion (e.g., Yang et al., 2010; Toyota et al., 2011; Falk and Sinnhuber, 2018), could be worthwhile implementing. The general model performance could also be improved by allowing for more plant functional types and phenologies than currently used or implementing an actual photosynthesis-based modeling of plants. ~~The photolysis- and chemical reaction computation as well as reaction rates shall also be revised in the future~~A more efficient parallelization of the code would enable computation on higher horizontal resolutions.

Code and data availability. The Oslo CTM3 shall be publicly available on git-hub under a MIT license in the future. Until then, access can be made granted under request. Model results can be made available under request.

Appendix A: Figures

Author contributions. Stefanie Falk has compiled the manuscript, finalized the implementation of the stomatal conductance in the EMEP-based dry deposition scheme of the Oslo CTM3, conducted the simulations, and analyzed and evaluated the results. Amund Søvde Haslerud has implemented the EMEP-based dry deposition scheme and wrote the respective documentation. Both authors contributed to the writing and discussion of the paper.

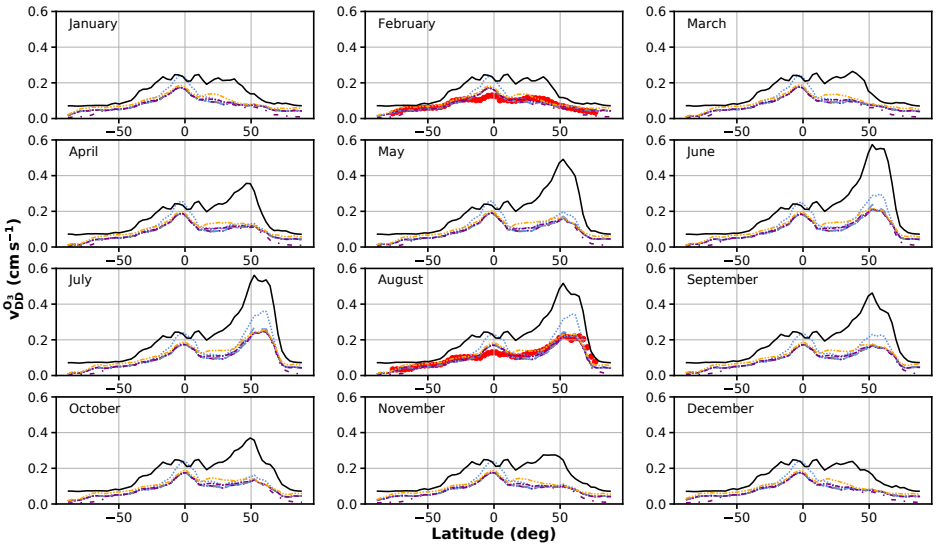

(a)

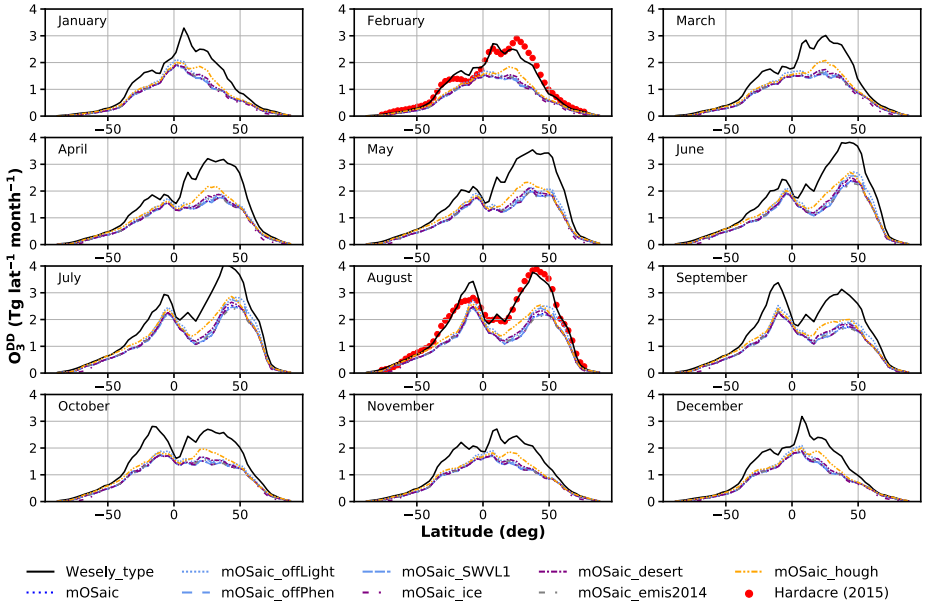

(b)

Figure A1. Comparison of the manifold of Oslo CTM3 integrations with respect to (a) Zonal average ozone dry deposition velocities; (b) Total annual amount of ozone removed from the atmosphere via dry deposition. The multi-model mean from the evaluation of TF HTAP models by Hardacre et al. (2015) is shown as a reference (where available).

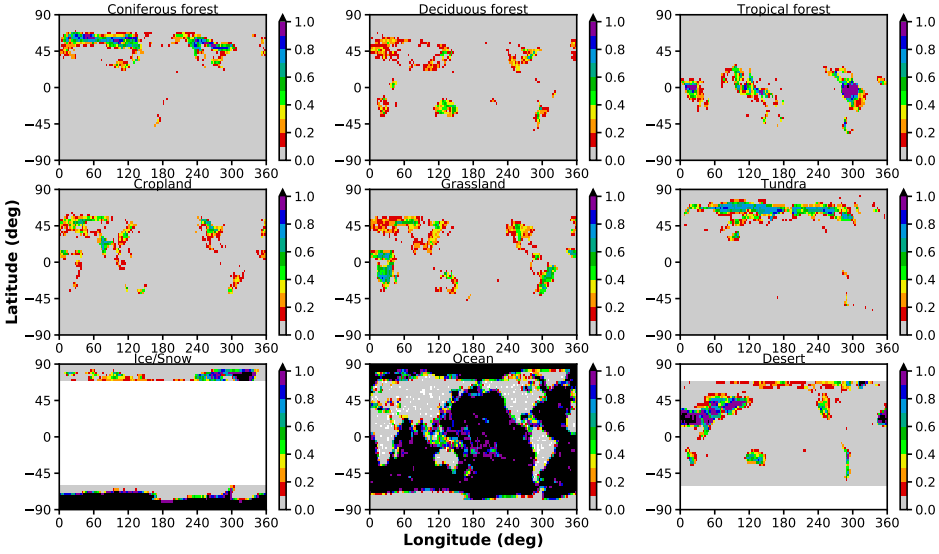

(a)

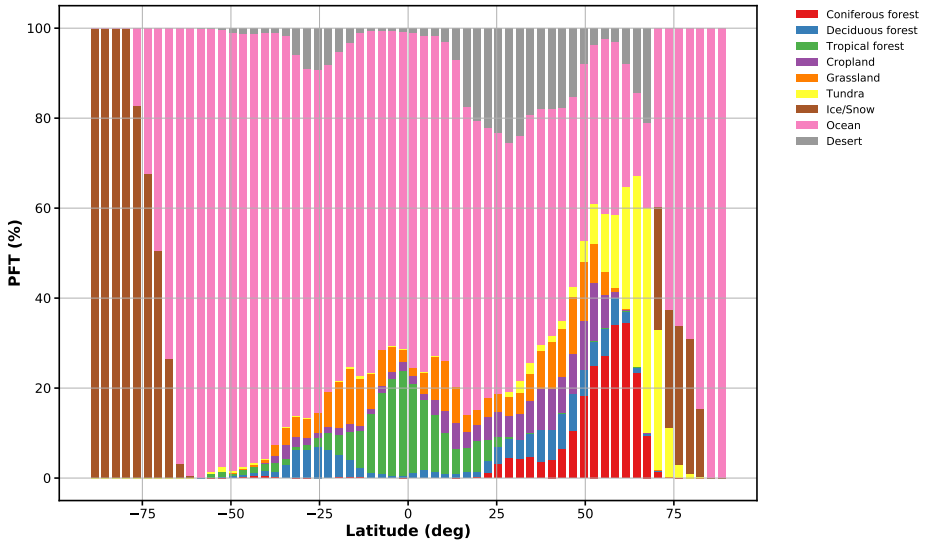

(b)

Figure B1. Partitioning of land surface types. (a) CLM 2 dynamic land surface types in $(0.5 \times 0.5)^\circ$ resolution; (b) Zonal distribution of land surface types.

Competing interests. The authors declare that they have no conflict of interest.

Acknowledgements. This work was supported by the Norwegian Research Council (NRC) through the project The double punch: Ozone and climate stresses on vegetation (268073).

The simulations were performed on resources provided by UNINETT Sigma2 – the National Infrastructure for High Performance Computing and Data Storage in Norway (project nn2806k).

The used Leaf Area Index (LAI) and roughness length (z_0) are available online from Oak Ridge National Laboratory Distributed Active Archive Center, Oak Ridge, Tennessee, U.S.A. (https://doi.org/10.3334/ORNLDAAC/970).

Community Emission Data System (CEDS) historical emission inventory is provided by the Joint Global Research Institute project (http://www.globalchange.umd.edu/ceds/.) Randerson, J.T., G.R. van der Werf, L. Giglio, G.J. Collatz, and P.S. Kasibhatla. 2018. Global Fire Emissions Database, Version 4, (GFEDv4). ORNL DAAC, Oak Ridge, Tennessee, USA. https://doi.org/10.3334/ORNLDAAC/1293 We would like to thank Prof. Frode Stordal (Section for Meteorology and Oceanography, University of Oslo) for discussions regarding early drafts of the manuscript~~as well as~~, Anne Fouilloux (scientific programmer at the same institute) for technical support as well as Olimpia Bruno (Karlsruhe Institute of Technology) and Franziska Hellmuth (University of Oslo) for valuable input regarding the aerodynamic resistance formulation. We would also like to thank the Center for International Climate Research (CICERO) for their support of this work.

References

Ainsworth, E. A.: Understanding and improving global crop response to ozone pollution, Plant J., 90, 886–897, https://doi.org/10.1111/tpj.13298, 2017.

Anav, A., Liu, Q., De Marco, A., Proietti, C., Savi, F., Paoletti, E., and Piao, S.: The role of plant phenology in stomatal ozone flux modeling, Glob. Change Biol., 24, 235–248, https://doi.org/10.1111/gcb.13823, https://onlinelibrary.wiley.com/doi/abs/10.1111/gcb.13823, 2017.

Anderson, M. C., Norman, J. M., Meyers, T. P., and Diak, G. R.: An analytical model for estimating canopy transpiration and carbon assimilation fluxes based on canopy light-use efficiency, Agr. Forest Meteorol., 101, 265–289, https://doi.org/10.1016/S0168-1923(99)00170-7, 2000.

Ball, J., Woodrow, I., and Berry, J.: Progress in Photosynthesis Research, chap. A Model Predicting Stomatal Conductance and its Contribution to the Control of Photosynthesis under Different Environmental Conditions, Springer, Dordrecht, 1987.

Barrie, L. A., Bottenheim, J. W., Schnell, R. C., Crutzen, P. J., and Rasmussen, R. A.: Ozone destruction and photochemical reactions at polar sunrise in the lower Arctic atmosphere, Nature, 334, 138–141, https://doi.org/10.1038/334138a0, 1988.

Bottenheim, J. W. and Chan, E.: A trajectory study into the origin of spring time Arctic boundary layer ozone depletion, J. Geophys. Res.-Atmos., 111, https://doi.org/10.1029/2006JD007055, 2006.

Bottenheim, J. W., Gallant, A. G., and Brice, K. A.: Measutements of NOy Species and O-3 at 82-Degrees-N Latitude, Geophys. Res. Lett., 13, 113–116, https://doi.org/10.1029/GL013i002p00113, 1986.

Buckley, T. N.: Modeling Stomatal Conductance, Plant Physiol., 174, 572–582, https://doi.org/10.1104/pp.16.01772, 2017.

Charnock, H.: Wind stress on a water surface, Q. J. Roy. Meteorol. Soc., 81, 639–640, https://doi.org/10.1002/qj.49708135027, https://rmets.onlinelibrary.wiley.com/doi/abs/10.1002/qj.49708135027, 1955.

Chuwah, C., van Noije, T., van Vuuren, D. P., Stehfest, E., and Hazeleger, W.: Global impacts of surface ozone changes on crop yields and land use, Atmos. Environ., 106, 11–23, https://doi.org/10.1016/j.atmosenv.2015.01.062, 2015.

Derwent, R. G., Parrish, D. D., Galbally, I. E., Stevenson, D. S., Doherty, R. M., Naik, V., and Young, P. J.: Uncertainties in models of tropospheric ozone based on Monte Carlo analysis: Tropospheric ozone burdens, atmospheric lifetimes and surface distributions, Atmos. Environ., 180, 93–102, https://doi.org/10.1016/j.atmosenv.2018.02.047, 2018.

Emberson, L. D., for Monitoring, C. P., of the Long Range Transmission of Air Pollutants in Europe, E., meteorologiske institutt, N., and Meteorological Synthesizing Centre-West (Oslo, N.: Towards a Model of Ozone Deposition and Stomatal Uptake Over Europe, EMEP/MSC-W Note, Norwegian Meteorological Institute, https://books.google.no/books?id=hj_ntgAACAAJ, 2000.

Erisman, J. W., Van Pul, A., and Wyers, P.: Parametrization of Surface-Resistance for the Quantification of Atmospheric Deposition of Acidifying Pollutants and Ozone, Atmos. Environ., 28, 2595–2607, https://doi.org/10.1016/1352-2310(94)90433-2, 1994.

Falk, S. and Sinnhuber, B.-M.: Polar boundary layer bromine explosion and ozone depletion events in the chemistry-climate model EMAC v2.52: implementation and evaluation of AirSnow algorithm, Geosci. Model Dev., 11, 1115–1131, https://doi.org/10.5194/gmd-11-1115-2018, 2018.

Falk, S., Sinnhuber, B.-M., Krysztofiak, G., Jöckel, P., Graf, P., and Lennartz, S. T.: Brominated VSLS and their influence on ozone under a changing climate, Atmos. Chem. Phys., 17, 11 313–11 329, https://doi.org/10.5194/acp-17-11313-2017, https://www.atmos-chem-phys.net/17/11313/2017/, 2017.

Fleming, Z. L., Doherty, R. M., von Schneidemesser, E., Malley, C. S., Cooper, O. R., Pinto, J. P., Colette, A., Xu, X., Simpson, D., Schultz, M. G., Lefohn, A. S., Hamad, S., Moolla, R., Solberg, S., and Feng, Z.: Tropospheric Ozone Assessment Re-

port: Present-day ozone distribution and trends relevant to human health, ELEMENTA-SCIENCE OF THE ANTHROPOCENE, 6, https://doi.org/10.1525/elementa.273, 2018.

Fu, Y., Zhang, H., Dong, W., and Yuan, W.: Comparison of Phenology Models for Predicting the Onset of Growing Season over the Northern Hemisphere, Plos One, 9, https://doi.org/10.1371/journal.pone.0109544, 2014a.

Fu, Y. H., Piao, S., Zhao, H., Jeong, S.-J., Wang, X., Vitasse, Y., Ciais, P., and Janssens, I. A.: Unexpected role of winter precipitation in determining heat requirement for spring vegetation green-up at northern middle and high latitudes, Glob. Change Biol., 20, 3743–3755, https://doi.org/10.1111/gcb.12610, 2014b.

Garratt, J. R.: The Atmospheric Boundary Layer, University Press, Cambridge, 1992.

Gaudel, A., Cooper, O. R., Ancellet, G., Barret, B., Boynard, A., Burrows, J. P., Clerbaux, C., Coheur, P. F., Cuesta, J., Cuevas, E., Doniki, S., Dufour, G., Ebojie, F., Foret, G., Garcia, O., Granados-Munoz, M. J., Hannigan, J. W., Hase, F., Hassler, B., Huang, G., Hurtmans, D., Jaffe, D., Jones, N., Kalabokas, P., Kerridge, B., Kulawik, S., Latter, B., Leblanc, T., Le Flochmoen, E., Lin, W., Liu, J., Liu, X., Mahieu, E., McClure-Begley, A., Neu, J. L., Osman, M., Palm, M., Petetin, H., Petropavlovskikh, I., Querel, R., Rahpoe, N., Rozanov, A., Schultz, M. G., Schwab, J., Siddans, R., Smale, D., Steinbacher, M., Tanimoto, H., Tarasick, D. W., Thouret, V., Thompson, A. M., Trickl, T., Weatherhead, E., Wespes, C., Worden, H. M., Vigouroux, C., Xu, X., Zeng, G., and Ziemke, J.: Tropospheric Ozone Assessment Report: Present-day distribution and trends of tropospheric ozone relevant to climate and global atmospheric chemistry model evaluation, ELEMENTA-SCIENCE OF THE ANTHROPOCENE, 6, https://doi.org/10.1525/elementa.291, 2018.

GEIA-ACCENT emission data portal: POET, online, Global CO emissions (1990–2000), http://accent.aero.jussieu.fr/database_table_inventories.php, 2003.

Guenther, A., Karl, T., Harley, P., Wiedinmyer, C., Palmer, P. I., and Geron, C.: Estimates of global terrestrial isoprene emissions using MEGAN (Model of Emissions of Gases and Aerosols from Nature), Atmos. Chem. Phys., 6, 3181–3210, https://doi.org/10.5194/acp-6-3181-2006, 2006.

Güsten, H., Heinrich, G., Mönnich, E., Sprung, D., Weppner, J., Ramadan, A. B., Ezz El-din, M. R. M., Ahmed, D. M., and Hassan, G. K. Y.: On-line measurements of ozone surface fluxes: Part II. Surface-level ozone fluxes onto the sahara desert, Atmos. Environ., 30, 911–918, https://doi.org/10.1016/1352-2310(95)00270-7, 1996.

Hardacre, C., Wild, O., and Emberson, L.: An evaluation of ozone dry deposition in global scale chemistry climate models, Atmos. Chem. Phys., 15, 6419–6436, https://doi.org/10.5194/acp-15-6419-2015, 2015.

Helmig, D., Ganzeveld, L., Butler, T., and Oltmans, S. J.: The role of ozone atmosphere-snow gas exchange on polar, boundary-layer tropospheric ozone - a review and sensitivity analysis, Atmos. Chem. Phys., 7, 2007.

Helmig, D., Lang, E. K., Bariteau, L., Boylan, P., Fairall, C. W., Ganzeveld, L., Hare, J. E., Hueber, J., and Pallandt, M.: Atmosphere-ocean ozone fluxes during the TexAQS 2006, STRATUS 2006, GOMECC 2007, GasEx 2008, and AMMA 2008 cruises, J. Geophys. Res.-Atmos., 117, https://doi.org/10.1029/2011JD015955, 2012.

Hinze, J. O.: Turbulence, p. 790, McGraw-Hill Series in Mechanical Engineering, McGraw-Hill, New York, 1975.

Hoesly, R. M., Smith, S. J., Feng, L., Klimont, Z., Janssens-Maenhout, G., Pitkanen, T., Seibert, J. J., V., L., Andres, R. J., Bolt, R. M., Bond, T. C., Dawidowski, L., Kholod, N., Kurokawa, J., Li, M., Liu, L., Lu, Z., Moura, M. C. P., O'Rourke, P. R., and Zhang, Q.: Historical (1750-2014) anthropogenic emissions of reactive gases and aerosols from the Community Emissions Data System (CEDS), Geosci. Model Dev., 11, 369–408, https://doi.org/10.5194/gmd-11-369-2018, 2018.

Hoshika, Y., Katata, G., Deushi, M., Watanabe, M., Koike, T., and Paoletti, E.: Ozone-induced stomatal sluggishness changes carbon and water balance of temperate deciduous forests, Sci. Rep.-UK, 5, https://doi.org/10.1038/srep09871, 2015.

Hossaini, R., Patra, P. K., Leeson, A. A., Krysztofiak, G., Abraham, N. L., Andrews, S. J., Archibald, A. T., Aschmann, J., Atlas, E. L., Belikov, D. A., Bönisch, H., Carpenter, L. J., Dhomse, S., Dorf, M., Engel, A., Feng, W., Fuhlbrügge, S., Griffiths, P. T., Harris, N. R. P., Hommel, R., Keber, T., Krüger, K., Lennartz, S. T., Maksyutov, S., Mantle, H., Mills, G. P., Miller, B., Montzka, S. A., Moore, F., Navarro, M. A., Oram, D. E., Pfeilsticker, K., Pyle, J. A., Quack, B., Robinson, A. D., Saikawa, E., Saiz-Lopez, A., Sala, S., Sinnhuber, B.-M., Taguchi, S., Tegtmeier, S., Lidster, R. T., Wilson, C., and Ziska, F.: A multi-model intercomparison of halogenated very short-lived substances (TransCom-VSLS): linking oceanic emissions and tropospheric transport for a reconciled estimate of the stratospheric source gas injection of bromine, Atmos. Chem. Phys., 16, 9163–9187, https://doi.org/10.5194/acp-16-9163-2016, http://www.atmos-chem-phys.net/16/9163/2016/, 2016.

Hough, A. M.: Development of a 2-Dimensional Global Tropospheric Model - Model Chemistry, J. Geophys. Res.-Atmos., 96, 7325–7362, https://doi.org/10.1029/90JD01327, 1991.

Hu, L., Jacob, D. J., Liu, X., Zhang, Y., Zhang, L., Kim, P. S., Sulprizio, M. P., and Yantosca, R. M.: Global budget of tropospheric ozone: Evaluating recent model advances with satellite (OMI), aircraft (IAGOS), and ozonesonde observations, Atmos. Environ., 167, 323–334, https://doi.org/10.1016/j.atmosenv.2017.08.036, 2017.

IPCC - Intergovernmental Panel on Climate Change: Climate Change 2013: The Physical Science Basis, 2013.

Jarvis, P. G.: The interpretation of the variations in leaf water potential and stomatal conductance found in canopies in the field, Philos. T. Roy. Soc. B., 273, 593–610, https://doi.org/10.1098/rstb.1976.0035, http://rstb.royalsocietypublishing.org/content/273/927/593, 1976.

Jin, L., Loisy, A., and Brown, N.: Role of meteorological processes in ozone responses to emission controls in California's San Joaquin Valley, J. Geophys. Res.-Atmos., 118, 8010–8022, https://doi.org/10.1002/jgrd.50559, 2013.

Levis, S. and Bonan, G. B.: Simulating springtime temperature patterns in the community atmosphere model coupled to the community land model using prognostic leaf area, J. Climate, 17, 4531–4540, https://doi.org/10.1175/3218.1, 2004.

Luhar, A. K., Galbally, I. E., Woodhouse, M. T., and Thatcher, M.: An improved parameterisation of ozone dry deposition to the ocean and its impact in a global climate-chemistry model, Atmos. Chem. Phys., 17, 3749–3767, https://doi.org/10.5194/acp-17-3749-2017, 2017.

Luhar, A. K., Woodhouse, M. T., and Galbally, I. E.: A revised global ozone dry deposition estimate based on a new two-layer parameterisation for air-sea exchange and the multi-year MACC composition reanalysis, Atmos. Chem. Phys., 18, 4329–4348, https://doi.org/10.5194/acp-18-4329-2018, 2018.

Lund, M. T., Myhre, G., Haslerud, A. S., Skeie, R. B., Griesfeller, J., Platt, S. M., Kumar, R., Myhre, C. L., and Schulz, M.: Concentrations and radiative forcing of anthropogenic aerosols from 1750 to 2014 simulated with the Oslo CTM3 and CEDS emission inventory, Geoscientific Model Development, 11, 4909–4931, https://doi.org/10.5194/gmd-11-4909-2018, https://www.geosci-model-dev.net/11/4909/2018/, 2018.

MACC-II Consortium: MACC Reanalysis of Global Atmospheric Composition (2003-2012), https://atmosphere.copernicus.eu/catalogue#/, Copernicus Atmosphere Monitoring Service (CAMS), 2011.

Matyssek, R., Wieser, G., Calfapietra, C., de Vries, W., Dizengremel, P., Ernst, D., Jolivet, Y., Mikkelsen, T. N., Mohren, G. M. J., Le Thiec, D., Tuovinen, J. P., Weatherall, A., and Paoletti, E.: Forests under climate change and air pollution: Gaps in understanding and future directions for research, Environ. Pollut., 160, 57–65, https://doi.org/10.1016/j.envpol.2011.07.007, 2012.

Mills, G., Sharps, K., Simpson, D., Pleijel, H., Broberg, M., Uddling, J., Jaramillo, F., Davies, W. J., Dentener, F., Van den Berg, M., Agrawal, M., Agrawal, S. B., Ainsworth, E. A., Büker, P., Emberson, L., Feng, Z., Harmens, H., Hayes, F., Kobayashi, K., Paoletti, E., and Van Dingenen, R.: Ozone pollution will compromise efforts to increase global wheat production, Glob. Change Biol., 24, 3560–3574, https://doi.org/10.1111/gcb.14157, https://onlinelibrary.wiley.com/doi/abs/10.1111/gcb.14157, 2018.

Mills, G., Harmens, H., Hayes, F., Pleijel, H., Büker, P., González-Fernandéz, I., Alonso, R., Bender, J., Bergmann, E. Bermejo, V., Braun, S., Danielsson, H., Gerosa, G., Grünhage, L., Karlsson, P. E., Marzuoli, R., Schaub, M., and Simpson, D.: ICP Mapping Manual - Chapter III: Mapping Critical Levels for Vegetation, International Cooperative Programme on Effects of Air Pollution on Natural Vegetation and Crops, https://icpmapping.org/Latest_update_Mapping_Manual, minor edits OCT 2017, 2017.

Mills, G., Pleijel, H., Malley, C. S., Sinha, B., Cooper, O. R., Schultz, M. G., Neufeld, H. S., Simpson, D., Sharps, K., Feng, Z., Gerosa, G., Harmens, H., Kobayashi, K., Saxena, P., Paoletti, E., Sinha, V., and Xu, X.: Tropospheric Ozone Assessment Report: Present-day tropospheric ozone distribution and trends relevant to vegetation, ELEMENTA-SCIENCE OF THE ANTHROPOCENE, 6, https://doi.org/10.1525/elementa.302, 2018.

Monks, P. S., Archibald, A. T., Colette, A., Cooper, O., Coyle, M., Derwent, R., Fowler, D., Granier, C., Law, K. S., Mills, G. E., Stevenson, D. S., Tarasova, O., Thouret, V., von Schneidemesser, E., Sommariva, R., Wild, O., and Williams, M. L.: Tropospheric ozone and its precursors from the urban to the global scale from air quality to short-lived climate forcer, Atmos. Chem. Phys., 15, 8889–8973, https://doi.org/10.5194/acp-15-8889-2015, 2015.

Monteith, J. L.: Principles of Environmental Physics, Edward Arnold, London, 1973.

Oltmans, S. J.: Surface Ozone Measurements In Clean-Air, J. Geophys. Res.-Oceans Atmos., 86, 1174–1180, https://doi.org/10.1029/JC086iC02p01174, 1981.

Otero, N., Sillmann, J., Mar, K. A., Rust, H. W., Solberg, S., Andersson, C., Engardt, M., Bergstrom, R., Bessagnet, B., Colette, A., Couvidat, F., Cuvelier, C., Tsyro, S., Fagerli, H., Schaap, M., Manders, A., Mircea, M., Briganti, G., Cappelletti, A., Adani, M., D'Isidoro, M., Pay, M.-T., Theobald, M., Vivanco, M. G., Wind, P., Ojha, N., Raffort, V., and Butler, T.: A multi-model comparison of meteorological drivers of surface ozone over Europe, Atmos. Chem. Phys., 18, 12 269–12 288, https://doi.org/10.5194/acp-18-12269-2018, 2018.

Pozzer, A., Joeckel, P. J., Sander, R., Williams, J., Ganzeveld, L., and Lelieveld, J.: Technical note: the MESSy-submodel AIRSEA calculating the air-sea exchange of chemical species, Atmos. Chem. Phys., 6, 5435–5444, 2006.

Schaap, M., Cuvelier, C., Hendriks, C., Bessagnet, B., Baldasano, J. M., Colette, A., Thunis, P., Karam, D., Fagerli, H., Graff, A., Kranenburg, R., Nyiri, A., Pay, M. T., Rouil, L., Schulz, M., Simpson, D., Stern, R., Terrenoire, E., and Wind, P.: Performance of European chemistry transport models as function of horizontal resolution, Atmos. Environ., 112, 90–105, https://doi.org/10.1016/j.atmosenv.2015.04.003, 2015.

Schnell, J. L., Prather, M. J., Josse, B., Naik, V., Horowitz, L. W., Cameron-Smith, P., Bergmann, D., Zeng, G., Plummer, D. A., Sudo, K., Nagashima, T., Shindell, D. T., Faluvegi, G., and Strode, S. A.: Use of North American and European air quality networks to evaluate global chemistry–climate modeling of surface ozone, Atmospheric Chemistry and Physics, 15, 10 581–10 596, https://doi.org/10.5194/acp-15-10581-2015, https://www.atmos-chem-phys.net/15/10581/2015/, 2015.

Seinfeld, J. H. and Pandis, S. N.: Atmospheric Chemistry and Physics: From Air Pollution to Climate Change, chap. 19, John Wiley & Sons, New York, 2nd edn., 2006.

Simpson, D., Tuovinen, J. P., Emberson, L., and Ashmore, M. R.: Characteristics of an ozone deposition module II: Sensitivity analysis, Water Air Soil Poll., 143, 123–137, https://doi.org/10.1023/A:1022890603066, 2003.

Simpson, D., Benedictow, A., Berge, H., Bergstrom, R., Emberson, L. D., Fagerli, H., Flechard, C. R., Hayman, G. D., Gauss, M., Jonson, J. E., Jenkin, M. E., Nyiri, A., Richter, C., Semeena, V. S., Tsyro, S., Tuovinen, J.-P., Valdebenito, A., and Wind, P.: The EMEP MSC-W chemical transport model - technical description, Atmos. Chem. Phys., 12, 7825–7865, https://doi.org/10.5194/acp-12-7825-2012, 2012.

Sindelarova, K., Granier, C., Bouarar, I., Guenther, A., Tilmes, S., Stavrakou, T., Muller, J. F., Kuhn, U., Stefani, P., and Knorr, W.: Global data set of biogenic VOC emissions calculated by the MEGAN model over the last 30 years, Atmos. Chem. Phys., 14, 9317–9341, https://doi.org/10.5194/acp-14-9317-2014, 2014.

Sitch, S., Cox, P. M., Collins, W. J., and Huntingford, C.: Indirect radiative forcing of climate change through ozone effects on the land-carbon sink, Nature, 448, 791–U4, https://doi.org/10.1038/nature06059, 2007.

Søvde, O. A., Prather, M. J., Isaksen, I. S. A., Berntsen, T. K., Stordal, F., Zhu, X., Holmes, C. D., and Hsu, J.: The chemical transport model Oslo CTM3, Geosci. Model Dev., 5, 1441–1469, https://doi.org/10.5194/gmd-5-1441-2012, 2012.

Stevenson, D. S., Dentener, F. J., Schultz, M. G., Ellingsen, K., van Noije, T. P. C., Wild, O., Zeng, G., Amann, M., Atherton, C. S., Bell, N., Bergmann, D. J., Bey, I., Butler, T., Cofala, J., Collins, W. J., Derwent, R. G., Doherty, R. M., Drevet, J., Eskes, H. J., Fiore, A. M., Gauss, M., Hauglustaine, D. A., Horowitz, L. W., Isaksen, I. S. A., Krol, M. C., Lamarque, J.-F., Lawrence, M. G., Montanaro, V., Müller, J.-F., Pitari, G., Prather, M. J., Pyle, J. A., Rast, S., Rodriguez, J. M., Sanderson, M. G., Savage, N. H., Shindell, D. T., Strahan, S. E., Sudo, K., and Szopa, S.: Multimodel ensemble simulations of present-day and near-future tropospheric ozone, J. Geophys. Res.-Atmos., 111, 2005.

Tai, A. P. K., Martin, M. V., and Heald, C. L.: Threat to future global food security from climate change and ozone air pollution, Nat. Clim. Change, 4, 817–821, https://doi.org/10.1038/NCLIMATE2317, 2014.

Tang, H., Takigawa, M., Liu, G., Zhu, J., and Kobayashi, K.: A projection of ozone-induced wheat production loss in China and India for the years 2000 and 2020 with exposure-based and flux-based approaches, Glob. Change Biol., 19, 2739–2752, https://doi.org/10.1111/gcb.12252, 2013.

Toyota, K., McConnell, J. C., Lupu, A., Neary, L., McLinden, C. A., Richter, A., Kwok, R., Semeniuk, K., Kaminski, J. W., Gong, S. L., Jarosz, J., Chipperfield, M. P., and Sioris, C. E.: Analysis of reactive bromine production and ozone depletion in the Arctic boundary layer using 3-D simulations with GEM-AQ: inference from synoptic-scale patterns, Atmos. Chem. Phys., 11, 3949–3979, https://doi.org/10.5194/acp-11-3949-2011, 2011.

Toyota, K., McConnell, J. C., Staebler, R. M., and Dastoor, A. P.: Air-snowpack exchange of bromine, ozone and mercury in the springtime Arctic simulated by the 1-D model PHANTAS - Part 1: In-snow bromine activation and its impact on ozone, Atmos. Chem. Phys., 14, 4101–4133, https://doi.org/10.5194/acp-14-4101-2014, 2014.

Tuovinen, J. P., Ashmore, M. R., Emberson, L. D., and Simpson, D.: Testing and improving the EMEP ozone deposition module, Atmos. Environ., 38, 2373–2385, https://doi.org/10.1016/j.atmosenv.2004.01.026, Workshop on the Development and Application of New Methods of Ozone Risk Assessment for Europe, Hindas, SWEDEN, NOV, 2002, 2004.

Warwick, N. J., Pyle, J. A., Carver, G. D., Yang, X., Savage, N. H., O'Connor, F. M., and Cox, R. A.: Global modeling of biogenic bromocarbons, J. Geophys. Res.-Atmos., 111, https://doi.org/10.1029/2006JD007264, 2006.

Wesely, M. L.: Parameterization Of Surface Resistances To Gaseous Dry Deposition In Regional-Scale Numerical-Models, Atmos. Environ., 23, 1293–1304, https://doi.org/10.1016/0004-6981(89)90153-4, 1989.

WHO - World Health Organization: Health risks of ozone from long-range transboundary air pollution, 2008.

Wilson, R. C., Fleming, Z. L., Monks, P. S., Clain, G., Henne, S., Konovalov, I. B., Szopa, S., and Menut, L.: Have primary emission reduction measures reduced ozone across Europe? An analysis of European rural background ozone trends 1996-2005, Atmos. Chem. Phys., 12, 437–454, https://doi.org/10.5194/acp-12-437-2012, 2012.

Wittig, V. E., Ainsworth, E. A., Naidu, S. L., Karnosky, D. F., and Long, S. P.: Quantifying the impact of current and future tropospheric ozone on tree biomass, growth, physiology and biochemistry: a quantitative meta-analysis, Glob. Change Biol., 15, 396–424, https://doi.org/10.1111/j.1365-2486.2008.01774.x, 2009.

WMO - Global Ozone Research and Monitoring Project: Scientific Assessment of Ozone Depletion: 2014, 2014.

Wu, J.: Wind-Stress Coefficients Over Sea-Surface Near Neutral Conditions - A Revisit, J. Phys. Oceanogr., 10, 727–740, https://doi.org/10.1175/1520-0485(1980)010<0727:WSCOSS>2.0.CO;2, 1980.

Yang, X., Pyle, J. A., Cox, R. A., Theys, N., and Van Roozendael, M.: Snow-sourced bromine and its implications for polar tropospheric ozone, Atmos. Chem. Phys., 10, 7763–7773, https://doi.org/10.5194/acp-10-7763-2010, 2010.

Young, P. J., Archibald, A. T., Bowman, K. W., Lamarque, J.-F., Naik, V., Stevenson, D. S., Tilmes, S., Voulgarakis, A., Wild, O., Bergmann, D., Cameron-Smith, P., Cionni, I., Collins, W. J., Dalsøren, S. B., Doherty, R. M., Eyring, V., Faluvegi, G., Horowitz, L. W., Josse, B., Lee, Y. H., MacKenzie, I. A., Nagashima, T., Plummer, D. A., Righi, M., Rumbold, S. T., Skeie, R. B., Shindell, D. T., Strode, S. A., Sudo, K., Szopa, S., and Zeng, G.: Pre-industrial to end 21st century projections of tropospheric ozone from the Atmospheric Chemistry and Climate Model Intercomparison Project (ACCMIP), Atmos. Chem. Phys., 13, 2063–2090, https://doi.org/10.5194/acp-13-2063-2013, https://www.atmos-chem-phys.net/13/2063/2013/, 2013.

Ziska, F., Quack, B., Abrahamsson, K., Archer, S. D., Atlas, E., Bell, T., Butler, J. H., Carpenter, L. J., Jones, C. E., Harris, N. R. P., Hepach, H., Heumann, K. G., Hughes, C., Kuss, J., Krueger, K., Liss, P., Moore, R. M., Orlikowska, A., Raimund, S., Reeves, C. E., Reifenhaeuser, W., Robinson, A. D., Schall, C., Tanhua, T., Tegtmeier, S., Turner, S., Wang, L., Wallace, D., Williams, J., Yamamoto, H., Yvon-Lewis, S., and Yokouchi, Y.: Global sea-to-air flux climatology for bromoform, dibromomethane and methyl iodide, Atmos. Chem. Phys., 13, 8915–8934, https://doi.org/10.5194/acp-13-8915-2013, 2013.